JGR Planets

RESEARCH ARTICLE
10.1029/2023JE007804

Sands on Meridiani Planum, Mars

J. Kozakiewicz[1], M. Kania[2], D. Salata[2], and L. Nowak[1]

[1]Faculty of Physics, Astronomy, and Applied Computer Science, Jagiellonian University, Krakow, Poland, [2]Faculty of Geography and Geology, Institute of Geological Sciences, Jagiellonian University, Krakow, Poland

Key Points:

- Sediments on the plains are different from those at the Endeavour crater rim in terms of the shape and chemical composition of grains
- Medium size sands are not present on the plains but are trapped in craters, where they can form dunes
- Very coarse sand grains are currently transported by wind but have shorter transport path lengths than grains transported in the past

Supporting Information:

Supporting Information may be found in the online version of this article.

Correspondence to:

J. Kozakiewicz,
j.kozakiewicz@uj.edu.pl

Citation:

Kozakiewicz, J., Kania, M., Salata, D., & Nowak, L. (2023). Sands on Meridiani Planum, Mars. *Journal of Geophysical Research: Planets*, *128*, e2023JE007804. https://doi.org/10.1029/2023JE007804

Received 27 FEB 2023
Accepted 18 SEP 2023

Abstract The analyses of 184 sediment targets and more than 70,000 individual grains revealed that along the Opportunity rover traverse there are four distinct fractions of deposits related to different geomorphological settings: (a) dust mixed with very fine sand is common behind topographical obstacles, (b) fine sands are deposited in depressions, (c) very coarse sands occur in coarse-grained ripple fields, and (d) gravel dominates at the rims of craters and on bedrock as lag deposits. Medium size sands were not observed on the plains, but they can be trapped in relatively large craters, where they form dunes and are within coarse-grained ripples and transverse aeolian ridges (TARs). The fine sands show no regional variations in chemical composition and granulometry, as these sands are easily transported by wind. The very coarse sands vary in composition and shape between the plains and the Endeavour crater rim as their sources are local and their transport distances are short. On the plains, the gravel and the coarse sands are enriched in iron and characterized by higher roundness than the grains from the Endeavour crater rim. The source of iron-rich, rounded grains on the plains are hematite spherules that are eroded out of Burns formation rocks. The smallest, the best sorted, and the least rounded coarse sand samples are found on coarse-grained ripple crests. They are mainly composed of spherule fragments and their low roundness indicates shorter transport path lengths than those of grains transported in the past when coarse-grained ripples migrated.

Plain Language Summary The analyses of more than 70,000 individual grains revealed that there are four distinct types of sediments on Meridiani Planum: (a) dust mixed with very fine sand grains (diameter below 0.10 mm) are common behind topographical obstacles, (b) fine sand grains (diameters 0.10–0.25 mm) are deposited in depressions, (c) very coarse sand grains (diameters 1–2 mm) occur in coarse-grained ripple fields, and (d) gravel (diameters above 2 mm) dominates at the rims of craters and on bedrock. Deposits composed of medium sand grains (diameter 0.25–0.50 mm) were not observed on the surface of the plains, but they can be trapped in relatively large craters, where they form dunes and are within coarse-grained ripples and transverse aeolian ridges formed by wind. The fine sands show no regional variations, indicating that these sands are mixed on a regional scale by sand-driving winds. The very coarse sands vary between the plains and the Endeavour crater rim, as their sources are local, and they can be moved by wind only over short distances.

1. Introduction

Studies of aeolian sediments are crucial for our understanding of aeolian erosion and accumulation that shape the surface of Mars. Both the size and density of grains in bedforms help to determine the wind speeds necessary to initiate and maintain aeolian transport. The regional and local changes in the granulometry, shape, and chemical composition of grains help us to infer aeolian transport distances, sources of material, and erosion and accumulation zones.

The grains in aeolian sediments must be studied at a microscopic scale since particles carried by wind are small (μm- to mm-scale), and this can only be done using data collected by the Martian rovers. The NASA Mars Exploration Rover (MER) mission that ended in 2018 consisted of two rovers: Spirit and Opportunity (Arvidson et al., 2006, 2010, 2011; Squyres et al., 2006). This mission studied two locations: Gusev crater and Meridiani Planum. Although the sediment data from Spirit in Gusev crater were thoroughly investigated (see e.g., Cabrol et al., 2014; Karunatillake et al., 2010; McGlynn et al., 2011; Yingst et al., 2008), Meridiani Planum deposits along the Opportunity rover traverse were mostly studied only at the initial stage of the mission (Geissler et al., 2008; Golombek et al., 2010; Herkenhoff et al., 2004, 2008; Jerolmack et al., 2006; Soderblom et al., 2004; Sullivan et al., 2005; Weitz et al., 2006), and at the later stage of the mission some properties of the deposits were mentioned in a mission overview (Arvidson et al., 2011).

The Opportunity rover landed in the western part of Meridiani Planum (MP) in January 2004 (Squyres et al., 2004). Over 14 years (5111 sols), Opportunity traveled more than 45 km. Its mission ended in Perseverance Valley at the western rim of Endeavour crater (Figure 1). The Opportunity mission overview can be found in Arvidson et al. (2011) and Squyres et al. (2006). Opportunity acquired data on sands from various landforms, such as fine- and coarse-grained ripples, gravel-sand sheets, wind streaks, and sand shadows.

In terms of geomorphological and geological settings, the traverse of the Opportunity rover can be divided into two parts (Figure 1): plains and the rim of Endeavour crater. The surface of the plains is composed of sulfate-rich sandstones, called the Burns formation (Squyres et al., 2004), covered by gravel-sand sheets, and coarse-grained ripples. In Burns formation, rocks are embedded in mm-scale hematite-rich spherules. Since the spherules are more resistant to erosion than the Burn formation rocks' matrix, they cover the surface of MP as a component of gravel-sand sheets (Squyres et al., 2006). Endeavour crater's rim rises above the Burns formation's layers and comprises Matijevic and Shoemaker formation rocks of basaltic composition (Mittlefehldt et al., 2018) and covered by gravel-sand sheets and rock fragments.

Early studies on Meridiani Planum sediments proposed some constraints on aeolian transport (Jerolmack et al., 2006) and characterized deposits in various geomorphological settings (Weitz et al., 2006); however, it was not possible to study regional differences between the plains and the Endeavour crater rim because Opportunity only began its journey to the latter location after these publications. As presently more data are available and the mission to Meridiani Planum is completed, we present the results of the granulometric, geochemical, and size analyses of all sediments that were investigated by Opportunity. On the basis of these results, it was determined whether the source of grains was local and what the local aeolian transport constraints were, and a sediment formation model was inferred.

2. Data and Methods

The size and shape of grains in deposits on MP can be studied directly using the Opportunity panchromatic Microscopic Imager (MI, Herkenhoff et al., 2004), and the chemical composition of grains can be measured using the Alpha Particle X-ray Spectrometer (APXS, Rieder et al., 2004).

2.1. Image Data

The MI was a microscope camera located on the rover's arm. The size of each MI image was 1024x1024 px, and its physical size of field of view (FOV) at the best focus was about 32 mm, as its pixel scale was 31 μm per pixel (Herkenhoff et al., 2003). If multiple MI images of a given deposit were available, a mosaic was created using Adobe Photoshop. To study the surrounding of deposits, data from the rover panoramic cameras were used: the stereoscopic panchromatic images from the Navigation Camera (NAVCAM; Maki et al., 2003) and panchromatic or color image composites from the Panoramic Camera (PANCAM; Bell et al., 2003). To study deposits in a broader context, grains detected in the MI images were overlaid on the color PANCAM images. The color PANCAM and panchromatic NAVCAM images were also used to identify different deposits. To produce false color images, we used L2, L5, and L7 PANCAM filters (see Bell et al., 2003). The Front Hazard Avoidance Camera (FRONTCAM; Maki et al., 2003) was used to find the exact location of the MI and APXS targets. All image data were acquired from the Planetary Data System (PDS) Geosciences Node.

To detect individual grains in the MI images, we used the Particle Detection and Measurement (PADM) algorithm (Kozakiewicz, 2018) implemented in Wolfram Mathematica. This is a semi-automated tool that allows fast detection of individual grains. The algorithm uses three techniques of image segmentation: thresholding (binarization), edge detection, and watershed. In the thresholding, the input image is binarized using a predetermined or manually determined threshold to obtain a mask of particles. The edge detection approach is used for grains with well-defined edges as it detects sharp changes in the image brightness. In the watershed technique, marker-controlled segmentation is used to define boundaries between particles similar to boundaries between ridges on a topographic map. It can be used for detecting grains that are in contact or separated from each other. The algorithm has some limitations, and if its use was not possible (e.g., due to uneven illumination in images), we employed manual tracking of the inner contours of grains using Adobe Photoshop. The differences between these two approaches as well as the inaccuracies related to the photosieving were small (Text S1 in Supporting Information S1).

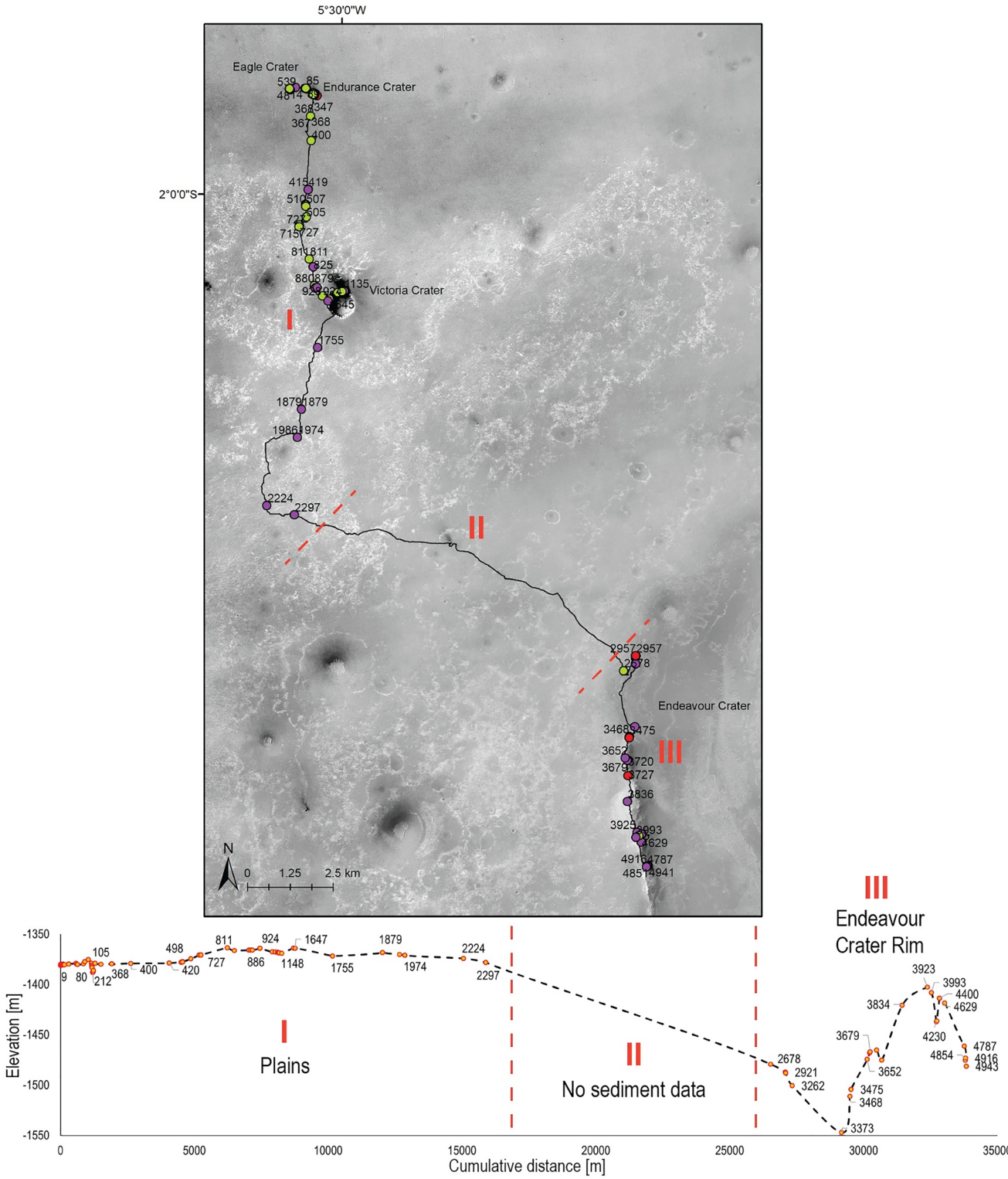

Figure 1. Top: traverse of the Opportunity rover (solid line) on MP (Mars Reconnaissance Orbiter Context Camera Image: G02_018846_1791_XN_00S005W, illumination from upper left, incident angle: 53.6°). Deposit targets studied only by MI—green dots, only by APXS—red dots, and by both instruments—purple dots. Numbers indicate sols. Bottom: targets' locations, black dashed line—distance between the studied targets (the cumulative distance between the targets is shorter than the actual rover traverse as drives to locations not related to the studied targets were omitted). "No sediment data" area describes a region that lacks sufficient sediment data for this study.

For grain shape analysis, only larger than 0.5 mm grains were included, as only for such grains the grain size to pixel size ratio was sufficient to correctly determine the contours of the grains. Also, particles that were smaller than 3 px (about 0.1 mm) in diameter were treated as unresolved in terms of size. We only studied clearly visible grains and did not analyze grains that were buried or truncated by the image border. To determine the roundness of the detected grains, we used an automatic algorithm by Zheng and Hryciw (2016) implemented in MathWorks MATLAB.

In this study, the Wentworth grain size classification is used (Wentworth, 1922). The diameter of a grain was defined as the diameter of a disk of the same area. The axes were calculated from the best-fitted ellipse computed from moment invariants. To study the shape of grains, we used circularity, aspect ratio, and roundness. The circularity was given by $4\pi A/P^2$, where A is the grain area and P is the perimeter of the grain. The aspect ratio was calculated as the ratio of the minor to major axis. The roundness was defined after Wadell (1932) and classified after Krumbein (1941). To characterize the size distribution of grains in a sample, four statistical moments were used: the mean, to characterize the grain size, the standard deviation (std), to indicate the sample sorting, the skewness, to find the asymmetry of the distribution, and the kurtosis, to measure the population outliers in the sample.

The number of fine sand particles in comparison to coarse sand particles is always underestimated, as only a part of small particles is clearly visible. On the other hand, smaller particles are always much more numerous than larger ones in a given FOV, and therefore finer particles easily overshadow coarser grains in particle size distributions (PSDs, Figure S1 in Supporting Information S1). Therefore, we statistically analyzed fine and coarse sands separately.

2.2. APXS Data

The chemical compositions of the samples were determined using data from the Alpha Particle X-ray spectrometer (APXS). The instrument measures both alpha particle-induced X-ray emission and X-ray fluorescence. When the APXS sensor head is in contact with the sample on the surface of a circular area of 38 mm diameter, the diameter of the field of view is 15 mm. The depth of measurement varies between 10 and 20 μm for Na and 50–100 μm for Fe. All measured elements were summed up to 100 wt.%. The detection limit is 0.1–1 wt.%, depending on the element (Rieder et al., 2004; Squyres et al., 2004). The data used were from the oxide abundance datasheet provided by the PDS Geosciences Node (Gellert, 2019).

The analyses were performed on the preselected set of samples. Sediment targets were analyzed with the exclusion of targets located in the tracks of the rover wheels, to minimize the risk of contamination by material from other locations. Furthermore, RAT-marked targets (targets disturbed by the rover Rock Abrasion Tool) were excluded. In total, 62 samples were analyzed.

2.3. Density Estimation

To estimate material density, a CIPW norm calculation was performed for the main elements (Verma et al., 2003) using GeoPyTool software (Yu et al., 2019). The obtained normative mineral composition (quartz, anorthite, diopside, hypersthene, albite, orthoclase, olivine, nepheline, apatite, ilmenite, and corundum) was then recalculated into the density contribution of each component and then summed up to obtain the total estimated density of the material. The mineral densities were based on Waples and Waples (2004 and references therein).

3. Results

3.1. General Characteristics of Targets

The investigated grains in the MI images were almost totally within a top layer of deposits. Although particles under the surface layers of deposits were sometimes visible in the MI images of the interiors of rover scuffs and tracks (Herkenhoff et al., 2008), it was not possible to quantitatively investigate these targets as they were often contaminated by material displaced by the rover wheels or falls of unconsolidated grains, and they were mostly poorly illuminated and blurred as their surfaces were typically perpendicular to the ground and very rough. Therefore, the presented quantitative results represent only the surface layer of a studied deposit and not the entire population of grains within the deposit. For the subsurface layers, some qualitative analyses are presented.

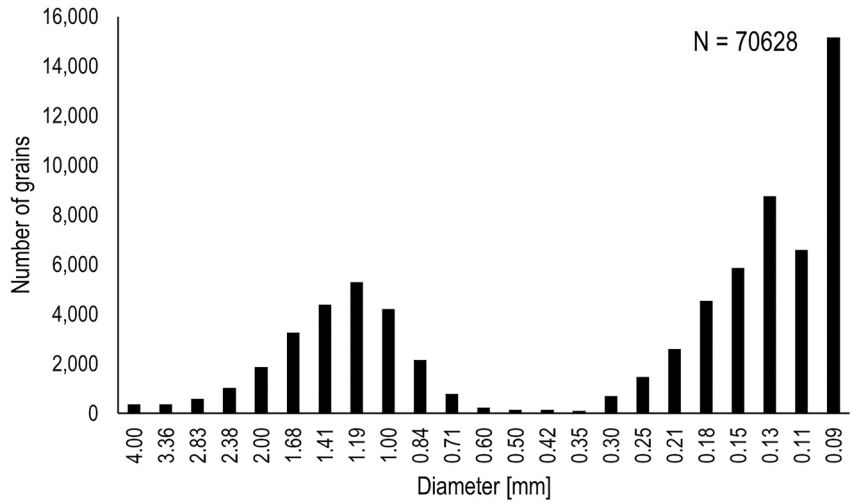

Figure 2. PSD for all samples. Fine sand grains (<0.25 mm) were not counted in samples with coarse sand and gravel, so the relative peaks' amplitudes between the coarser (>0.5 mm) and the finer fractions (<0.5 mm) cannot be directly compared. The values presented on the *x*-axis are the lower limits of the grain diameter range. The "0.09 mm" range in all PSD figures in this work includes only grains between 0.10 and 0.11 mm, as smaller than 0.10 mm grains cannot be studied due to the MI resolution limit. The "4 mm" range indicates grains larger than 4 mm.

The MI images can be divided into three groups of targets in terms of the occurrence of grains. The grains were related to regolith (soil) targets (Figure S2a in Supporting Information S1), but they were also present on rocks (bedrock, boulders, Figure S2b in Supporting Information S1), and on magnets (Figure S2c in Supporting Information S1) located on the rover body (Madsen et al., 2003). A sample was classified as a rock sample when grains in an image were at least partially deposited on a rocky surface. Along the traverse, 131 MI targets were classified as regolith targets, 39 as rock targets, and 10 as magnet targets (Table S1 in Supporting Information S1). Of the regolith targets, 52 were from bedforms: 42 from coarse-grained ripples, 3 from sand shadows, 2 from bright wind streaks, 2 from dark fine sand ripples, and 3 from bright fine sand ripples (Table S1 in Supporting Information S1). The locations of the investigated targets are presented in Figure 1. For the purpose of this study, if several MI targets with the same sediment type were obtained in nearby locations, they were combined into one sample for further analysis (Figure S3 in Supporting Information S1). On the other hand, if an MI target included various deposits in the same location, the target was divided into separate samples. Furthermore, if the sediments were disturbed by the rover wheels or characterized by too few particles to obtain a valid interpretation, they were not included in the final results. Therefore, the number of final samples (137, Table S2 in Supporting Information S1) is different from the number of MI targets (180, Table S1 in Supporting Information S1).

The numbers of MI targets and APXS targets are not equal, as there are some MI targets which were not measured or analyzed by APXS and vice versa. Moreover, the APXS data reflect the composition of the grains over the entire measurement area. Therefore, the results of the APXS analysis provide information not only about the grains, but also about the materials between the grains, while the MI image analysis can focus on selected grains (Figure S4 in Supporting Information S1).

3.2. Size and Shape of Grains

The entire population of grains larger than 0.1 mm has a bimodal distribution with two clearly visible peaks: one at about 0.13 mm and the second at about 1.20 mm (Figure 2), indicating that there are almost no medium sands on MP. The third peak at 0.10 mm represents only part of the population of smaller particles that were probably much more numerous but were not recognized due to the limited resolution of the MI images.

The deposits on MP can be divided into four fractions (Figure 3, Table 1): (a) dust and very fine sands (which may contain dust aggregates), (b) fine sands, (c) coarse and very coarse sands, and (d) gravel. In 11 cases, the number and non-uniformity of the particles did not allow classification to any of these four groups, and these 11 samples were classified as mixed fractions. Both very fine sand and dust (<0.1 mm in diameter) are below

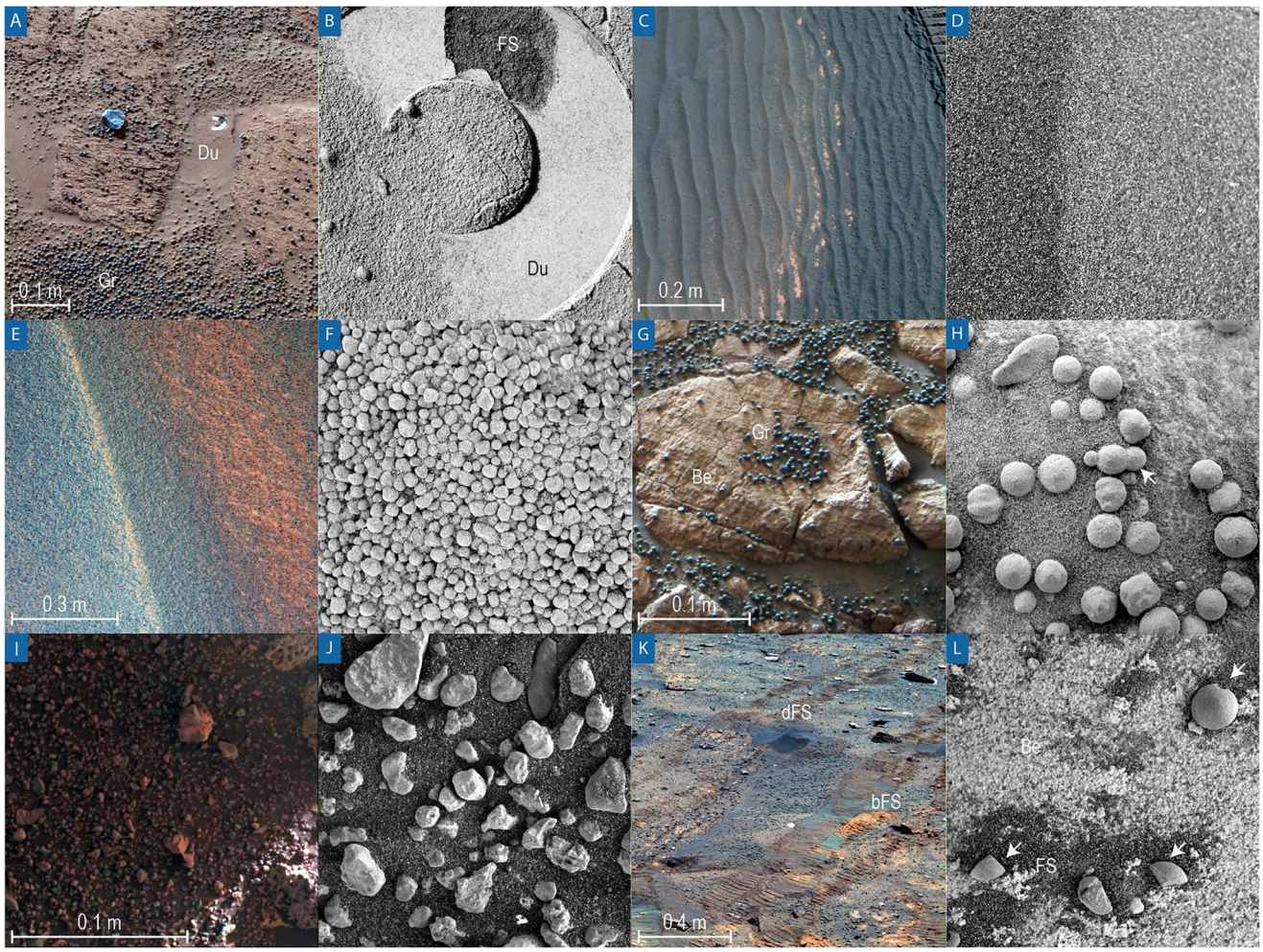

Figure 3. Types of deposits on MP. Du—dust and very fine sand, FS—fine sand, CS—coarse sand, Gr—gravel, Be—bedrock. (a) Dust and very fine sand with spherules (Gr) at the rim of Endurance crater (Pancam, sol 0123). (b) Close up of the sediment compressed by the Mössbauer contact plate. On the surface there is a thin layer of size fractions <0.1 mm, below which there is dark fine sand. Uncompressed material form aggregates (Herkenhoff et al., 2008; MI, sol 0123, "McDonnell"). (c) Dark fine sand in ripples on the floor of Eagle crater, with pink patches composed of grains <0.1 mm (Pancam, sol 0054), (d) Close up of fine sand in one of the ripples (MI, sol 0055, "Ripple Four"). (e) Very coarse sand on a ripple crest (the crest runs from upper left to lower right, Pancam, sol 0464). (f) Close up of very coarse sand on the ripple crest (MI, sol 0498, "NewFace"). (g) Spherules (Gr) on bedrock (Pancam, sol 0043). (h) Close up of spherules on bedrock; arrow indicates a triple spherule grain (MI, sol 0048, "BERT"). (i) Gravel on fine sand at the Endeavour crater rim (Pancam, sol 4938). (j) Close up of gravel at the Endeavour crater rim (MI, sol 4941, "Carizal"). (k) Bright and dark sands in Endurance crater (Pancam, sol 0294). (l) Spherule and fragments of spherules (white arrows) on bedrock in Endurance crater (MI, sol 0257, "Tilcho2"). All Pancam images are in enhanced color. All MI images are 3.2 × 3.2 cm.

the MI resolution limit. They are bright in panchromatic images and pinkish in false-color images (Figures 3a and 3b). There are two types of very fine and fine sands >0.1 mm (0.12–0.25 mm in diameter; Figure 3k): dark sand and bright sand. In false-color images, dark sand is dark gray, whereas bright sand is yellowish. In many places these two fine sands (Figure 3k) are mixed together; however, dark sand is always dominant (Figure 3c). Very coarse and coarse sands (Figures 3e and 3f) are bluish in false-color images and made up of spherical and angular grains. Gravel grains (Figures 3g–3j) can be divided into two categories: spherules (Figures 3g and 3h) bluish in false-color images and granules—angular grains in various colors but predominantly bluish (Figures 3i and 3j). These four fractions often occur simultaneously, but in different proportions. Some of these sands are more common in certain geomorphological settings (Figure 4, Table 1). On the magnets, only very fine and fine sand grains were deposited.

For all samples, the amount of grains, mean, median, minimum, and maximum diameters, as well as the skewness and kurtosis are presented in Table S2 of the Supporting Information S1. The mean and standard deviation for circularity, roundness, and aspect ratio, as well as the mean major and minor axes were calculated for coarse sands and gravel (Table S3 in Supporting Information S1).

Table 1
Deposits Along the Opportunity Traverse

	Dust & very fine sand	Fine sand	Coarse and very coarse sand	Gravel
Size	<0.1 mm	0.10–0.25 mm, *D*: 0.10 mm, 0.13 mm	0.5–2.0 mm, *D*: 1.20 mm	>2.0 mm, *D*: 2.00 mm
Shape	–	–	*C*: 0.79–0.93, *R*: 0.52–0.70	*C*: 0.75–0.90, *R*: 0.46–0.77
Enhanced color	Pinkish	Dark gray or yellowish	Bluish	Bluish
Typical locations on the surface	Leeward side of obstacles	Small depressions, leeward side of small obstacles	Coarse-grained ripple fields	Outcrops, crater rims, coarse-grained ripple troughs
Occurrence	Wind streaks, very fine sand ripples	Fine sand ripples, sand shadows, wind streaks	Coarse-grained ripples, lag deposits	Lag deposits

Note. *D*—typical diameter (see Figure 2), *C*—circularity range, *R*—roundness range. The grain size is given by the grain diameter. The gravel was investigated mainly up to 4 mm in diameter.

The results indicate that the skewness is positive for gravel and larger coarse sand grains, and negative for fine sands and smaller coarse sand particles (Figure 5b), due to enrichment in larger particles and depletion in smaller particles on MP, even if to some extent the smallest grains are slightly influenced by the image resolution, and the largest by the image FOV. The best sorted very coarse sands were deposits on coarse-grained ripple crests (Figure 5a). The least sorted are mixed samples, which were often close to a material source related to bedrock fragmentation (Figure 5c). It is worth mentioning that all mixed samples were located in the Endurance crater, except for "Albuquerque" from Endeavour crater. The coarse-grained ripple crests were enriched in smaller coarse sand grains at the expense of the ripple troughs (Figure 5d). The granulometric analysis for all sand samples and chosen gravel samples is presented in Figures 6–9.

3.3. Granulometry of Fine Sands

Dust and very fine sand grains were below the resolution of the MI images. However, fine sand and dust aggregates were visible in almost all MI images. Locations where dust and very fine sand dominate are wind streaks on the leeward side of obstacles, such as the crests of coarse-grained ripples or the rims of craters (Figure 4b). These finer fractions are also present beneath the surface of other deposits, which are clearly visible in rover tracks and scuffs (Figure 4a). Bright small (cm-scale wavelength) ripples, which were especially common in troughs between coarse-grained ripples located at the rims of relatively large craters, are at least partially composed of these grains (Figure 4c).

Fine sand grains were measured only where dust and dust aggregates were not dominant. Such sediments were found on rocks (bedrock, boulders), magnets, and within fine sand deposits (sand shadows, cm-scale wavelength dark fine sand ripples, deposits in bedrock fractures). To study fine sand deposits, we focused on images in which larger grains were very rare. If in the samples, larger individual grains (>0.5 mm in diameter) were present, they were removed from the statistical analysis. We classified 22 samples as fine sand samples and 5 samples as very fine sand samples. Only 4 samples ("LiverEatingJohnson," "QueenAdelaide," "Durango," "JosephCollin") were from Endeavour crater, and the rest from the plains.

The fine sands were located mainly in small depressions, such as impact craters (Figure 4e), shallow lineaments (Sullivan & Kok, 2017), and behind small obstacles, such as rocks. Fine sands formed sand ripples (Figures 3c and 4e) or sand shadows (Figure 4f). The analyzed sands were mostly of a bimodal distribution (Figure 6), with sorting from very good to moderately good (Table S2 in Supporting Information S1). The mean diameter and sorting of these samples did not depend on the location along the traverse or the type of a setting (Figure 10). Only samples deposited on bedrock are characterized by more variable kurtosis and skewness (Figure 10).

The filter and capture magnets' images were taken by the MI camera. The filter magnet was designed to capture the most magnetic particles and the capture magnet any magnetic particles (Madsen et al., 2003). The results do not indicate differences between grains deposited on those two magnets (Figures 6 and 10).

In some samples, an increase in the percentage of larger grains in the PSD can be partially related to the presence of aggregates of finer particles, but larger grains, 0.18 mm in diameter, are also often found, even on the magnets (see e.g., Filter from sol 0038 in Figure 6).

3.4. Granulometry of Very Coarse Sands

Coarse and very coarse sands were always mixed with fine sands and dust. However, to find differences between the coarse sand samples along the traverse, we did not include fine sands (<0.25 mm) in the analysis of the coarse sand samples. We classified 53 samples as very coarse sand samples and only 4 as coarse sand samples (Table S2 in Supporting Information S1). Of these 57 deposits, 29 were related to coarse-grained ripples (their crests, slopes, or troughs, Figures 4g and 4h). Other sediments were related to lag deposits found mainly within coarse-grained ripple fields or in craters, in settings such as on bedrock (Figure 3g), in rock fractures (Figure 4k), and within gravel-sand sheets (Figures 3i and 4a). Almost all coarse and very coarse sand samples were found on the plains, and only three at the Endeavour crater rim ("Amboy5," "Amboy11," "RockCreek," Figure 11).

The sands found on coarse-grained ripple slopes and crests were always very well or well sorted and unimodal in distribution. On the other hand, the sands in ripple troughs were only moderately well to well

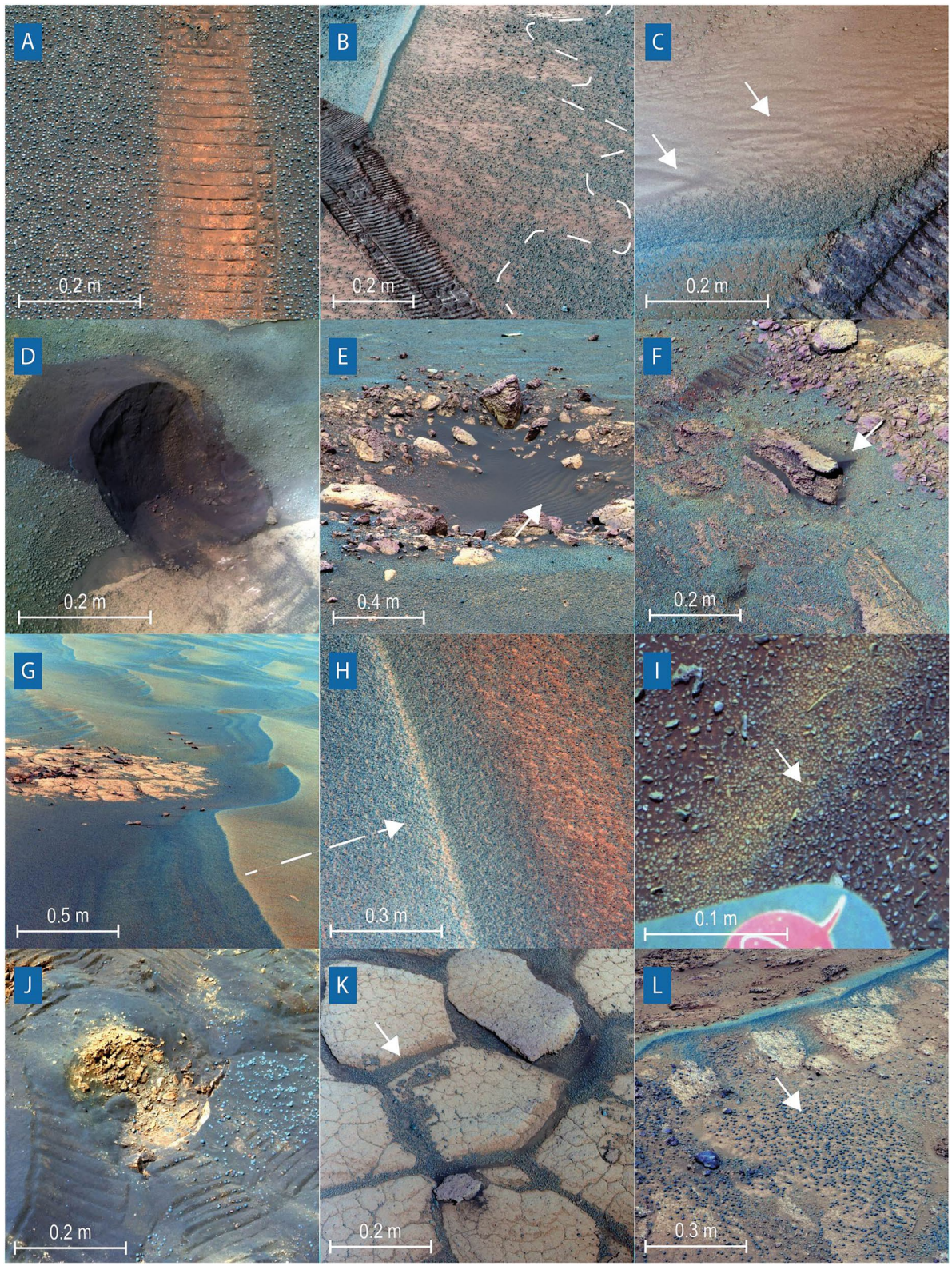

Figure 4.

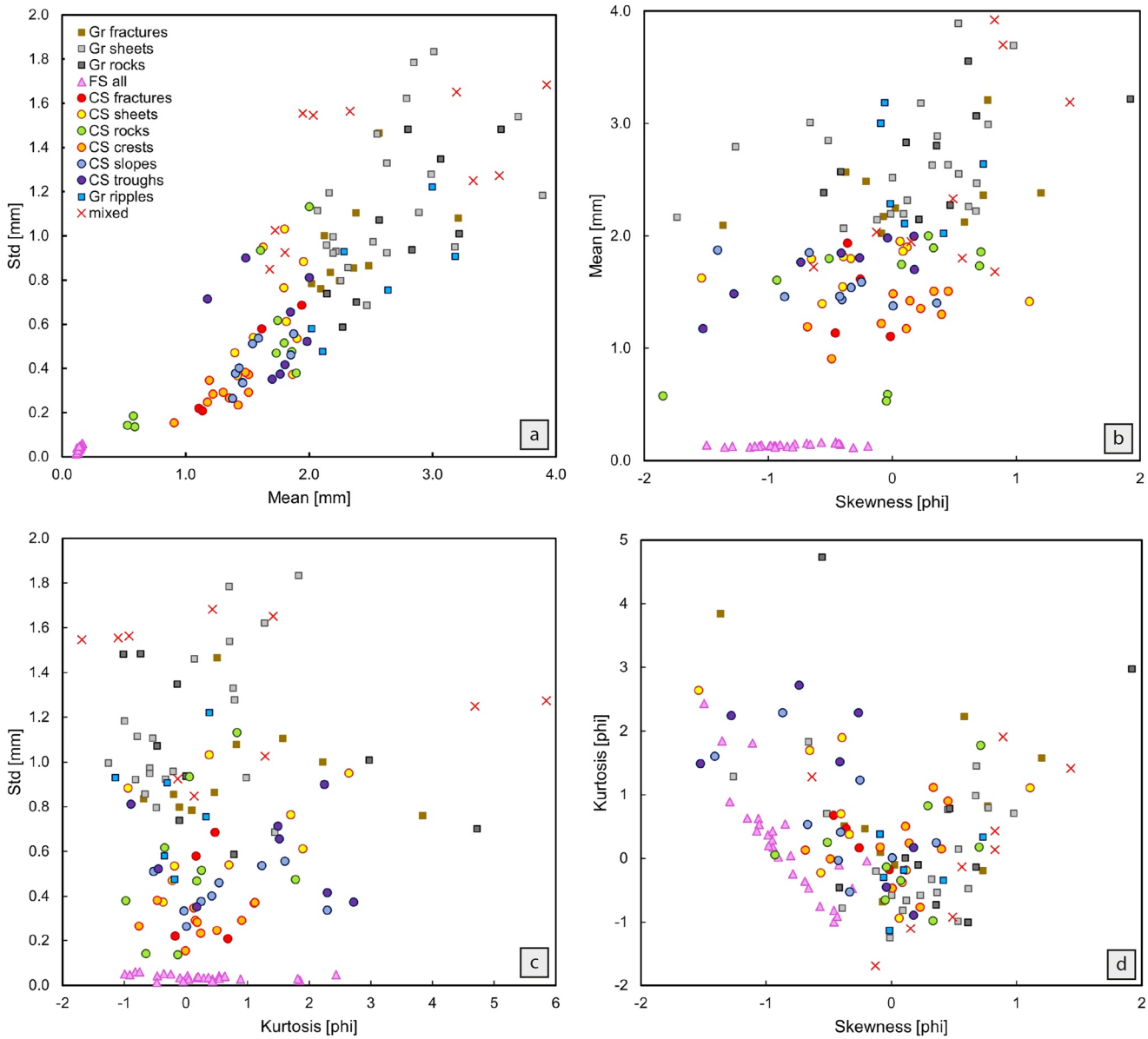

Figure 5. Size and distribution for all studied samples in various settings (sediments in bedrock fractures, sand-gravel sheets, on bedrock, coarse-grained ripple crests, slopes, and in coarse-grained ripple troughs). Gr—gravel, CS—coarse sand, FS—fine sand. (a) Mean diameter versus standard deviation (std). (b) Size versus skewness. (c) Standard deviation versus kurtosis. (d) Kurtosis versus skewness.

sorted. These sands were mostly unimodal, and the non-unimodal samples were related to spherules present in the samples ("Panaluu," "VailBeach"; Figure 8). The coarse sands found outside ripples were unimodal or bimodal and moderately well to very well sorted. Trimodal distributions were found only in four samples and in all of these cases it was due to the enrichment in spherules or their fragments ("Outfield," "Salamanca," "Branchwater," "SamiKai"; Figure 7).

Figure 4. Typical locations of deposits. All images are in enhanced color. Scale bars are representative of the central part of images. (a) Gravel-sand sheet with a rover track. The gravel is mostly composed of spherules (sol 1139). (b) Dust wind streak (area of the streak to the left of the dashed line) on the leeward side of a crater rim (sol 0060). (c) Bright small ripples (white arrows) near a coarse-grained ripple (bottom, sol 2953). (d) A rover scuff: under a thin layer of material composed mostly of spherules is a deep layer of fine sand (sol 1444). (e) Ripples in a crater with a floor covered by fine sand (sol 1160). (f) Sand shadows (made of fine sand) behind a rock (sol 3039). (g) Coarse-grained ripples (sol 2247). (h) Crest of a coarse-grained ripple made of very coarse sand (sol 0464). (i) Crest of coarse-grained ripple made of fine gravel (sol 3652). (j) Fragmentation of a rock from Burns Formation by the rover wheels generates yellowish sand and gravel grains (sol 0255). (k) Grains often concentrate in fractures in bedrock (sol 2314). (l) Lag deposit made of spherules (dark blue) near a crater rim indicated by the presence of a coarse-grained ripple (light blue, sol 2512).

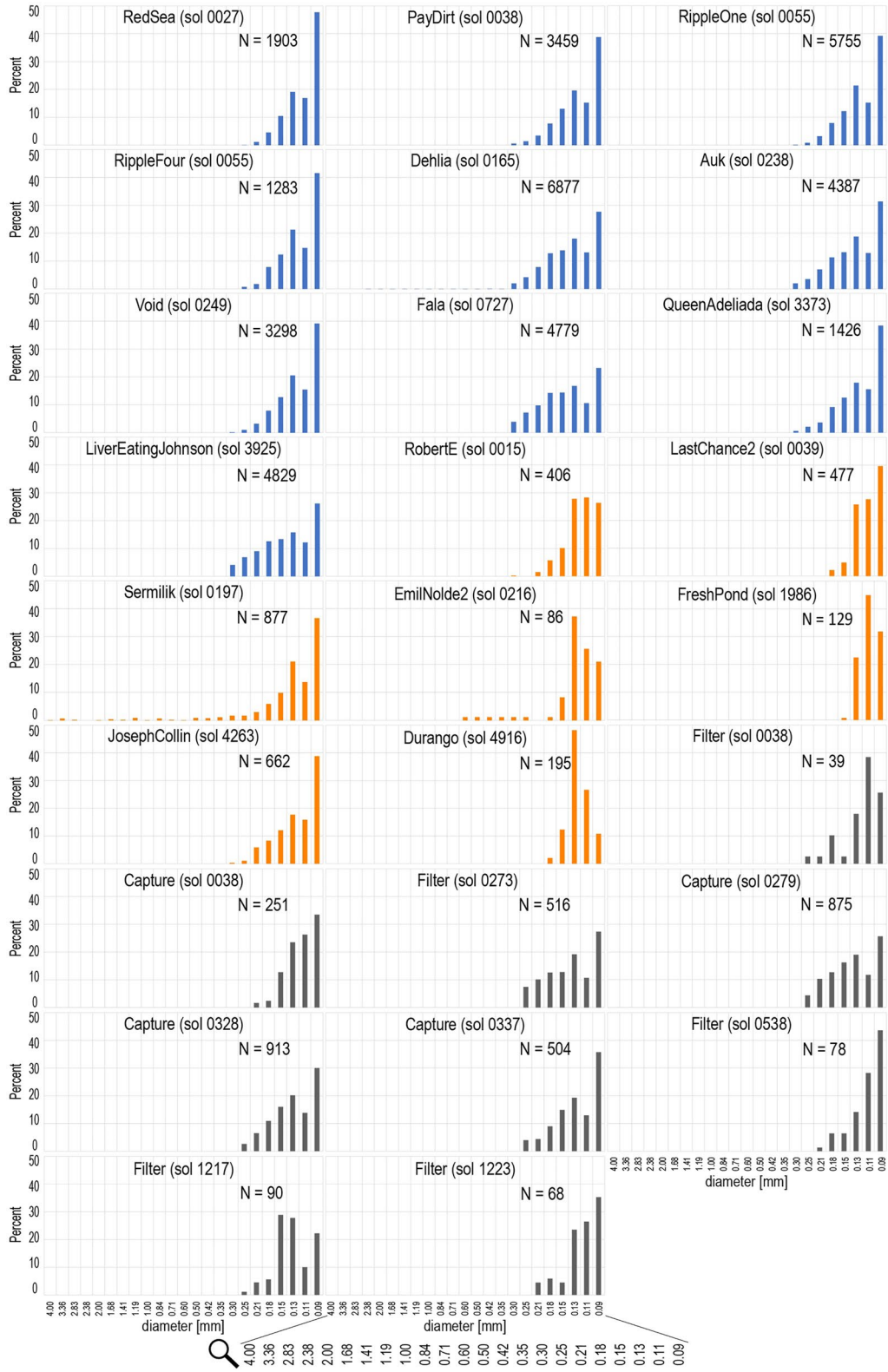

Figure 6. PSDs for fine and very fine sand samples. Blue—regolith samples, orange—rock samples, gray—magnet samples. N—number of grains.

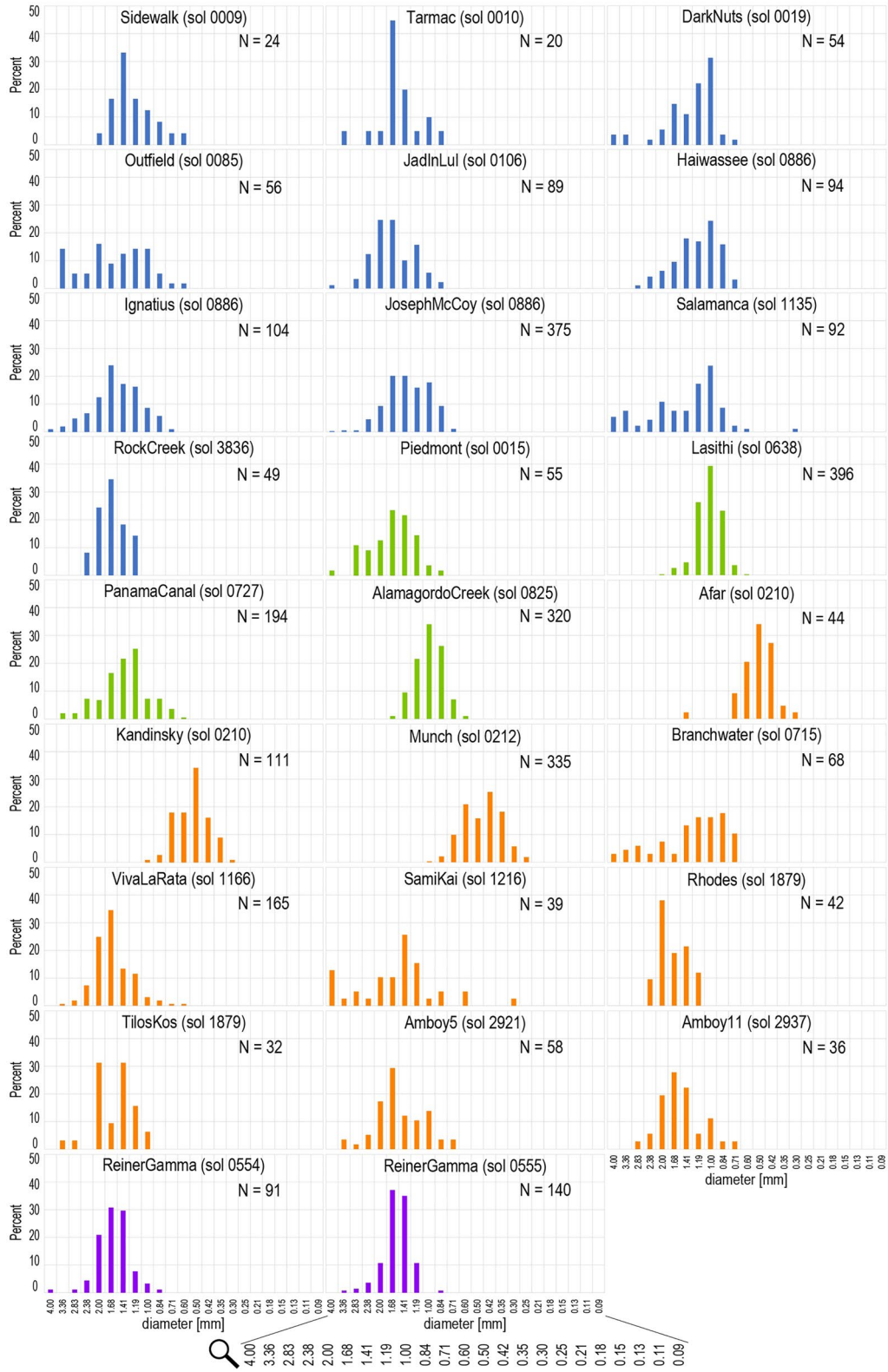

Figure 7. PSDs for very coarse and coarse sand samples. Blue—regolith samples, green—sediment in bedrock fractures, orange—rock samples, purple—coarse-grained ripple samples (troughs). N—number of grains.

Figure 8. PSDs for very coarse and coarse sand samples from coarse-grained ripples. Two bottom rows—samples from ripple troughs. N—number of grains.

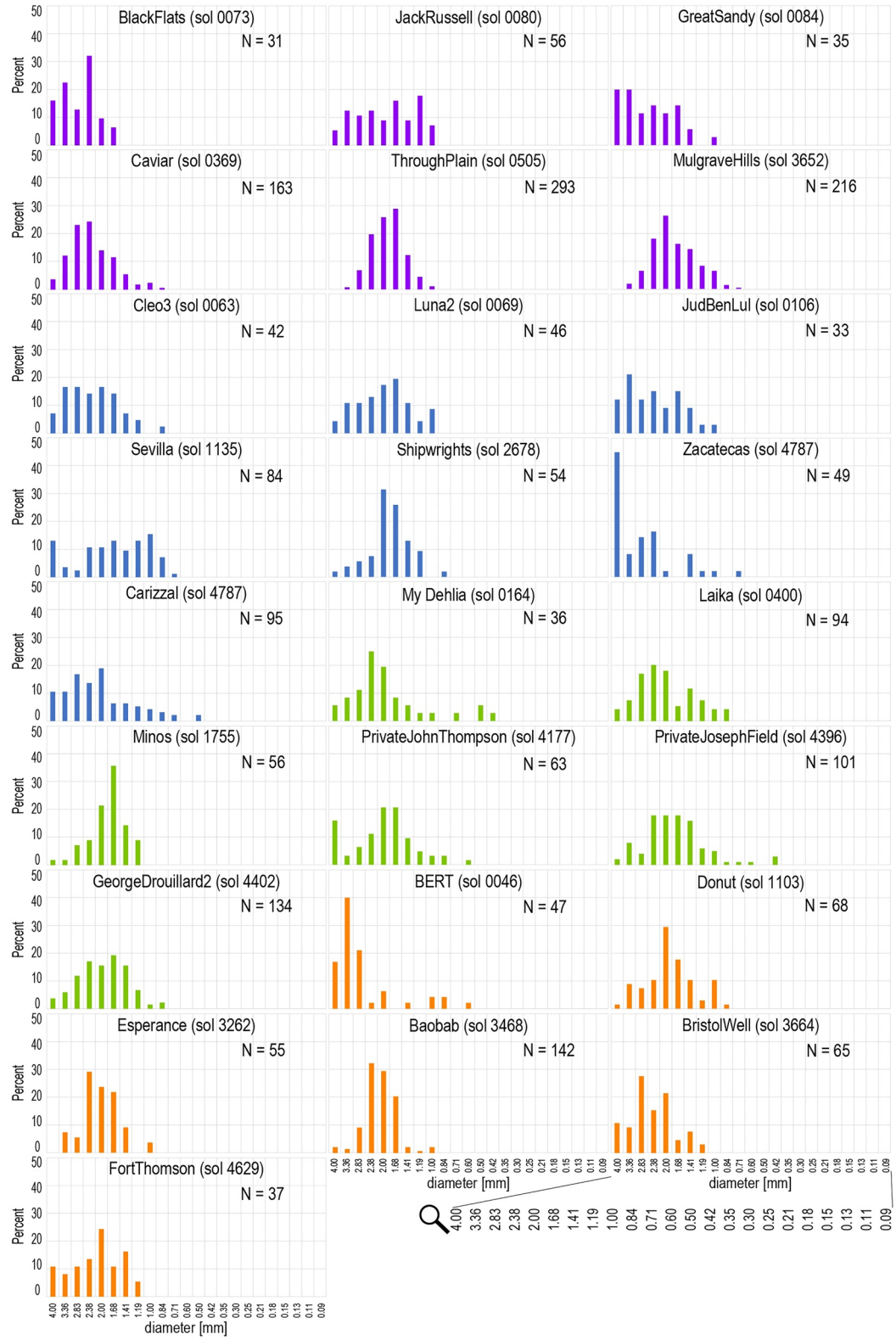

Figure 9. PSDs for chosen gravel samples. Purple—ripple samples, blue—gravel-sand sheet samples, green—sediments in bedrock fissures, and orange—rock samples. N—number of grains.

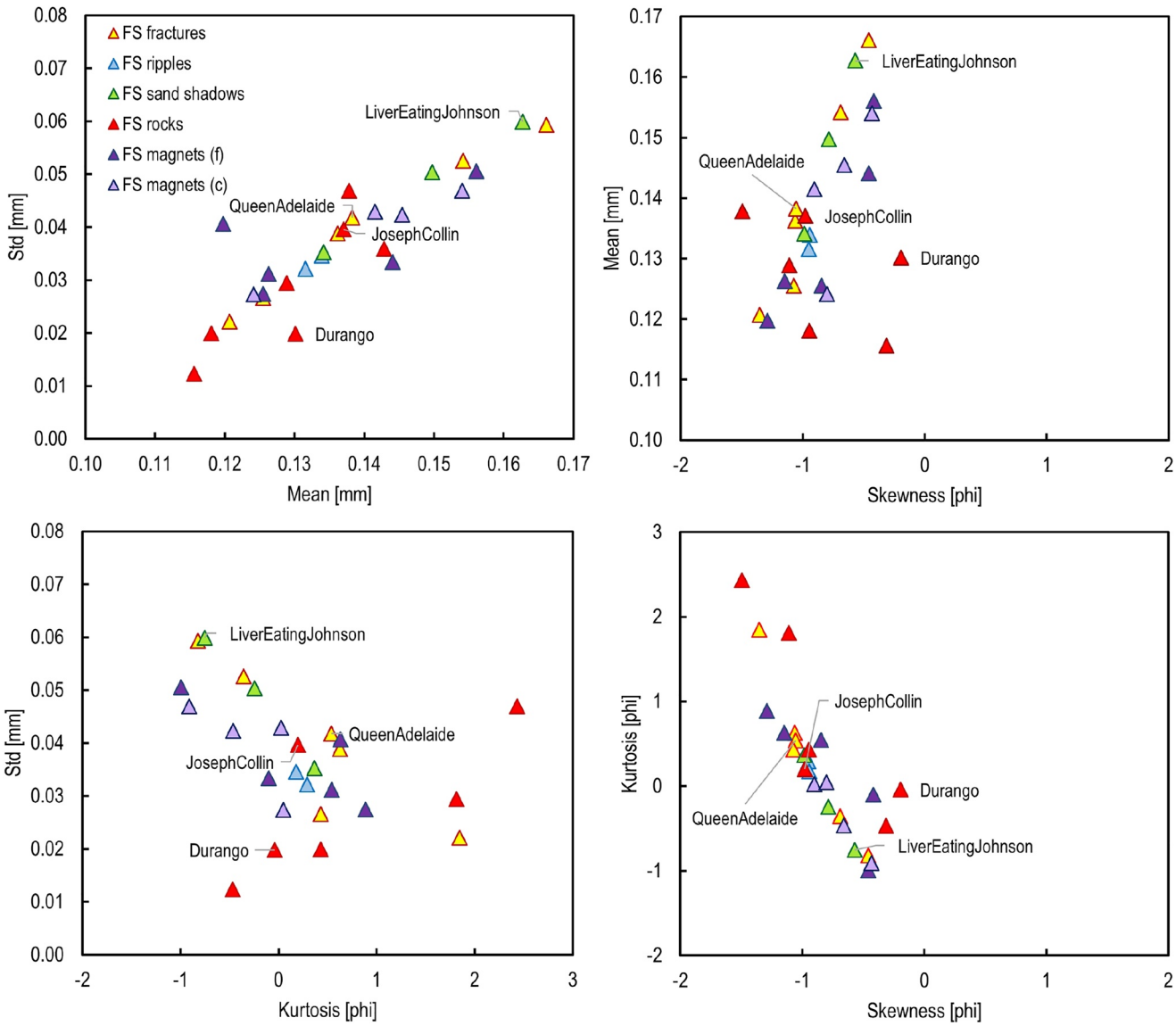

Figure 10. Size and distribution of fine sands in various settings (bedrock fractures, fine sand ripples, sand shadows, bedrock, and magnets: f—filter, c—capture). Samples from Endeavour crater are indicated by labels.

The mean diameter for all coarse sand samples was similar apart from four samples (Table S2 in Supporting Information S1): three of them were found inside Endurance crater (Afar, Kandinsky, Munch; see also Weitz et al., 2006) and one in Eagle crater ("Vanilla2," see also Weitz et al., 2006). The most striking examples are samples from the Endurance crater, which consist of not only coarse sand grains but also of medium sand grains that were not found elsewhere in such proportions. These three samples were from the lower part of the inner flank of the crater and were deposits on the same bedrock. The Eagle Crater sample was from a coarse-grained ripple crest. This irregular ripple in terms of shape (Figure S5 in Supporting Information S1) was also located on the inner flank of the crater. In this case, the small mean diameter is related to a high number of very well-sorted small spherules. These four samples are also characterized by the modal peak <1 mm. Beside these four samples, only one sample has a peak below 1 mm "CookiesNCream," which is from a trough of the irregular coarse-grained ripple in Eagle crater (the crest of which is represented by "Vanilla2," Figure S5 in Supporting Information S1). Most samples have the peak >1 mm, and only 10 samples at 1 mm (Figures 7 and 8). Of these 10 samples, two samples are the most interesting: "Lasithi" and "AlamogordoCreek," which are composed solely of very well sorted coarse sand particles. These two samples are from fractures in bedrock within coarse-grained ripple fields. The other six samples ("RippleCrest2b," "Mayberooz," "NewCrest," "TormentTrack," "Hawkins," and "Hall,"

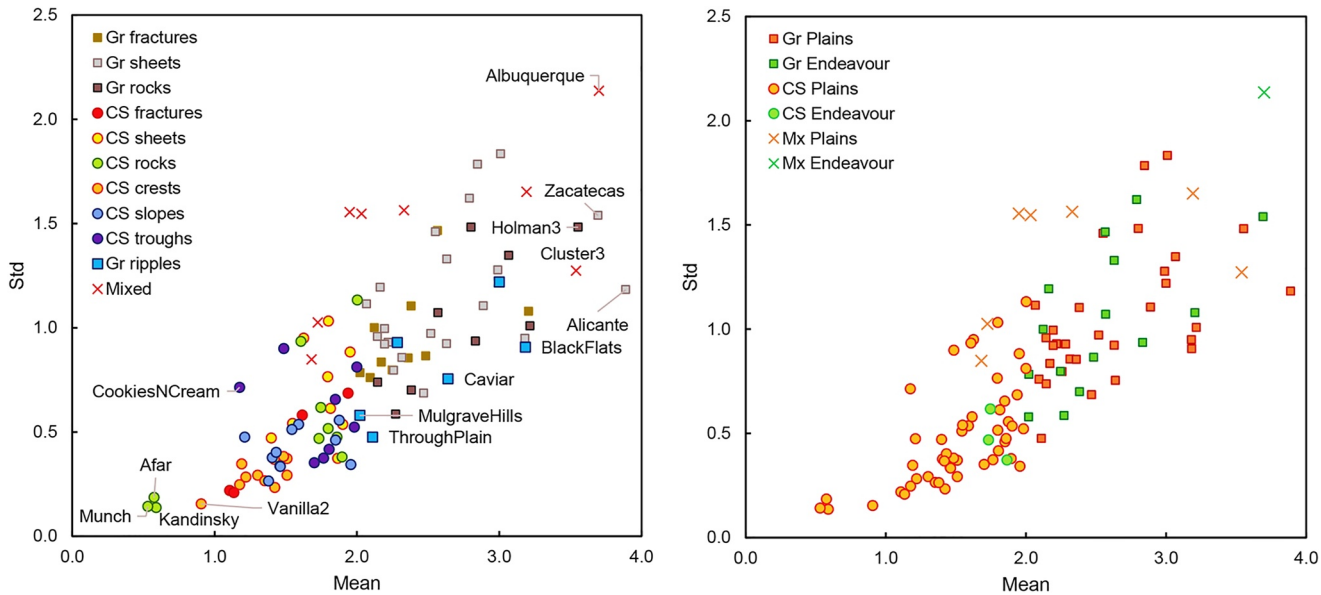

Figure 11. Size and sorting (in mm) of coarse sand and gravel: (on the left) in various settings: in gravel-sand sheets, on coarse-grained ripples, in bedrock fractures, on bedrock, (on the right) in two regions: plains and Endeavour crater.

Figure S5 in Supporting Information S1) were from very well or well-sorted material from slopes, crests, or troughs of coarse-grained ripples, and the last two samples from well-sorted gravel-sand sheets with a large proportion of coarse sand particles ("DarkNuts," "Haiwassee").

3.5. Granulometry of Gravel

Studying sand on MP is not possible without analyzing gravel particles. Gravel particles on MP are very common and create extensive gravel-sand sheets (Figures 3i and 4a), which are practically everywhere along the rover traverse. On the plains, gravel is mostly made up of spherules of various sizes (Figures 3g, 3h, and 3l). At the rim of Endeavour crater, gravel consists of granules and pebbles of various shapes and sizes (Figures 3i and 3j).

Some coarse-grained ripples are also composed of gravel particles (Figure 9). "MullgraveHills" sample is a gravel sample from a crest of a ripple located on the outer flank of the Endeavour crater. "Caviar" is from a slope and "ThroughPlain," "BlackFlats," "Great Sandy," and "JackRussell" are from a trough of coarse-grained ripples located on the plains. The last three samples are from small ripples and due to the small size of these ripples (8 cm wide) and their large spacing (50 cm), these three samples are more similar to gravel-sand sheet samples than to the samples from larger coarse-grained ripples (which have m-scale width and spacing).

Only 6 gravel samples are unimodal (Figure 9): three samples from the coarse-grained ripples ("MulgraveHills" "Caviar" and "ThroughPlain"), one sample from a fracture in bedrock on the plains ("Minos"), one sample from a gravel-sand sheet located around the rim of Endeavour crater ("Shipwrights"), and a sample found on bedrock at the rim of Endeavour crater ("Baobab").

There are at least three populations of spherules on MP: the smallest spherules (which are rare) with a mean diameter of approximately 1.0 mm, the medium size spherules with a mean diameter of 2.0 mm, and the largest spherules with a mean diameter greater than 4.0 mm. The largest spherule found in the MI images has a diameter of 7.6 mm. The common modal peak for the gravel samples with a mixture of coarse sand particles and gravel is at 2.0 mm, but the most typical modal peak for all gravel samples is >4.0 mm, which is the result of the frequent occurrence of larger particles in the samples.

3.6. Shape of Very Coarse Sand and Gravel Grains

The least rounded off all samples were coarse sand grains from ripples (Figure 12). More rounded were very coarse sand and gravel grains found in gravel-sand sheets, on bedrock, and in bedrock fractures. This can only

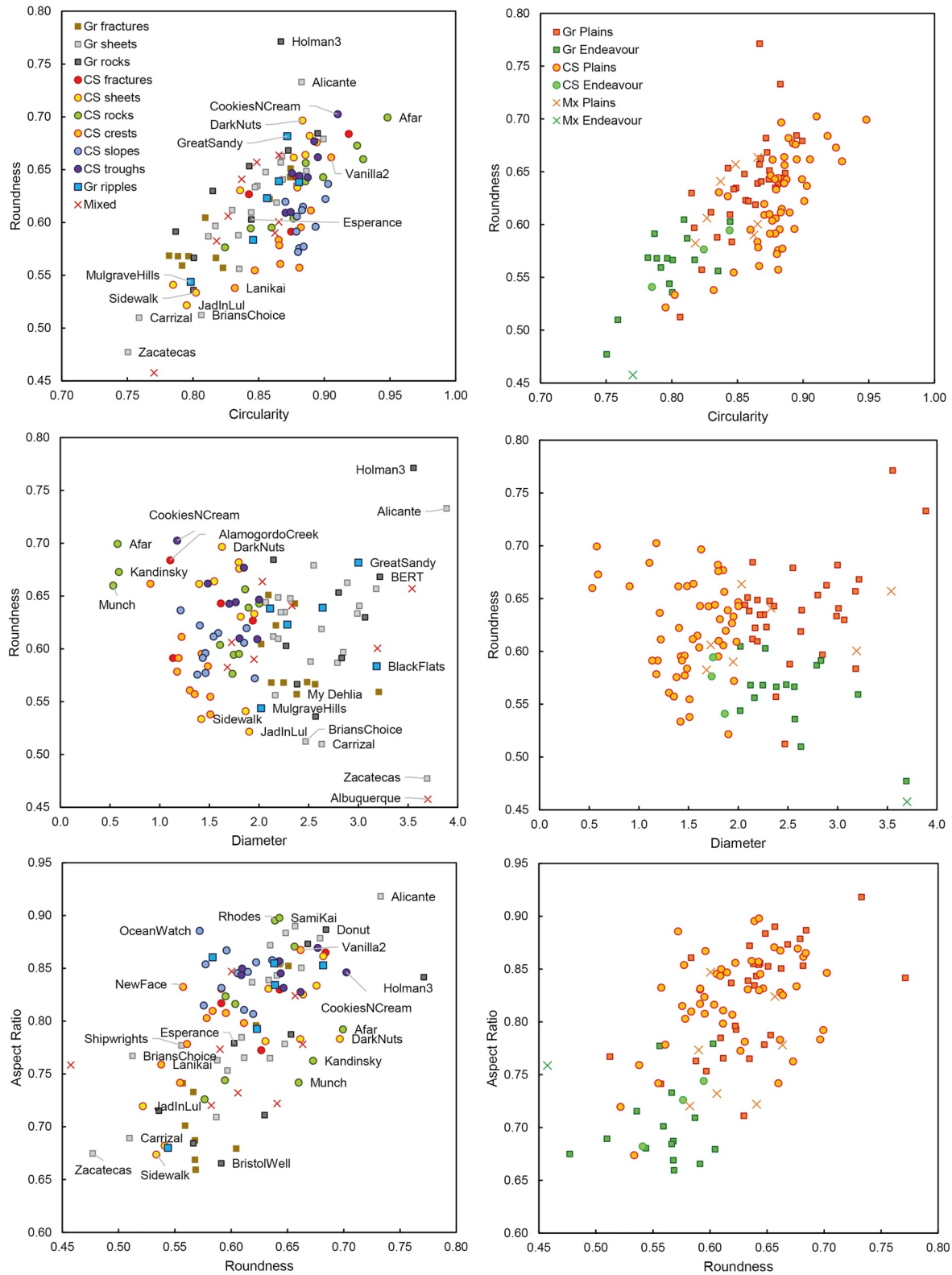

Figure 12. Shape and size (in mm) of very coarse sand and gravel: (on the left) in various settings and (on the right) in two regions: plains and Endeavour crater.

partially be explained by the presence of spherules. The only well-rounded sand sample from ripple crests was "Vanilla2," composed mainly of small spherules.

In the case of gravel samples, there is a positive correlation between circularity and roundness, apart from two samples composed mainly of spherules: "Holman3" and "Alicante" (Figure 12; Figure S6 in Supporting Information S1). The higher roundness of the gravel than of the sands is due to the higher percentage of spherules in the gravel samples. Spherules have higher roundness but lower circularity than sand grains. Some spherules can be double or even triple grains (Figure 3h), further decreasing their circularity.

Typically, the grains on the plains were more rounded, have larger circularity, and have a higher aspect ratio than grains at Endeavour crater (Figure 12). Only three samples from the plains: "JadInLul," "Sidewalk," and "BriansChoice" were less rounded. However, all of them were from the craters on the plains: the first was from Endurance crater and the other two from Eagle crater. The most rounded grains are related to gravel samples enriched in spherules such as "Holman3" or "Alicante."

3.7. Characteristics of Coarse-Grained Ripple Samples

For aeolian transport studies, the most important are samples from bedforms, and only one type of bedform dominates along the Opportunity traverse: coarse-grained ripples. The coarse-grained ripples are covered by an armor of very coarse sand particles, under which well-sorted fine sands form a ripple interior. These fine sands are similar to those observed elsewhere on MP (see e.g., Jerolmack et al., 2006). Although the sand in the ripple interiors was visible in a few MI images that showed the interiors of the rover scuffs, it was not possible to investigate these samples as they were contaminated by displaced material, poorly illuminated, or blurred. Therefore, in this work, we focus only on the ripple armoring layers, composed mainly of non-saltating coarser sand particles (e.g., coarse sands). These armoring layers were formed due to deflation of saltating size particles (e.g., fine sands), which led to coarsening of ripple surfaces.

Whenever possible, the rover acquired more than one sample from the same ripple to find differences in sediments within the ripple armoring layer (Figure 13f). From one ripple are (see Figure S5 in Supporting Information S1): "NewFace" (crest), "NewCrest" (subsurface layers beneath the crest) and from a neighboring similar ripple are "Flank1" (slope), "ThroughPlain" (trough), "CleatTab" and "TormentTrack" (both subsurface layers beneath the slope and surface layers on the slope, these two samples were disturbed by the rover wheels). From another ripple on the plains are (Figure S5 in Supporting Information S1): "RippleCrest2b" (crest) and "Caviar" (slope). Similarly, for 7 other ripples (Figure S5 in Supporting Information S1): "Lanikai" (crest) and "Panaluu" (trough); "Vanilla2" (crest) and "CookiesNCream" (trough); "Hawkins" (slope) and "Hall" (trough), "Norooz" (eastern side of the crest), "Mayberooz" (western side of the crest) and "Mobarek" (trough); "Isabella" (upper part of the upper slope) and "Marchena" (lower part of the upper slope), "PecosRiver" (upper slope) and "FortSumner" (lower part of the upper slope); "AegeanCrest" (crest) and "BlackFlats" (trough). Almost all the ripple samples were acquired from the plains, and only one from Endeavour crater ("Mulgrave Hills").

The grains in the coarse-grained ripple crests are mostly smaller than the grains in the coarse-grained ripple slopes, and the grains in the ripple slopes are mostly smaller than the grains in the ripple troughs (Figures 13e and 13f). Also, the best sorted (with the smallest standard deviation) are the sands on the ripple crests (Figure 13a). "MulgraveHill", a sample from the crest of a coarse-grained ripple located at Endeavour crater, is made up of larger grains than those on the ripples on the plains, although it is still well sorted (Figure 13a).

Almost all the coarse-grained ripple crest samples have positive skewness and the ripple slope and trough samples have negative skewness (Figure 13b). "Caviar" (slope sample) is also characterized by positive skewness, indicating that this gravel sample is enriched in sand particles (Figure 13b). The gravel samples from the ripple troughs are very similar and have zero skewness. Most of the coarse sand samples from the ripple troughs are leptokurtic, with negative skewness and poorer sorting (Figures 13a and 13b), indicating mixing with gravel and enrichment in coarser sand grains.

As mentioned above, the least rounded grains are on the coarse-grained ripple crests. Only one ripple crest sample ("Vanilla2") has a mean roundness greater than 0.65, but this sample is composed of small spherules. The samples from different parts of the same ripple have different roundness (Figure 13f). Even if the diameters of grains on the upper and lower slopes are similar, the roundness on the lower slope is higher than that on the upper

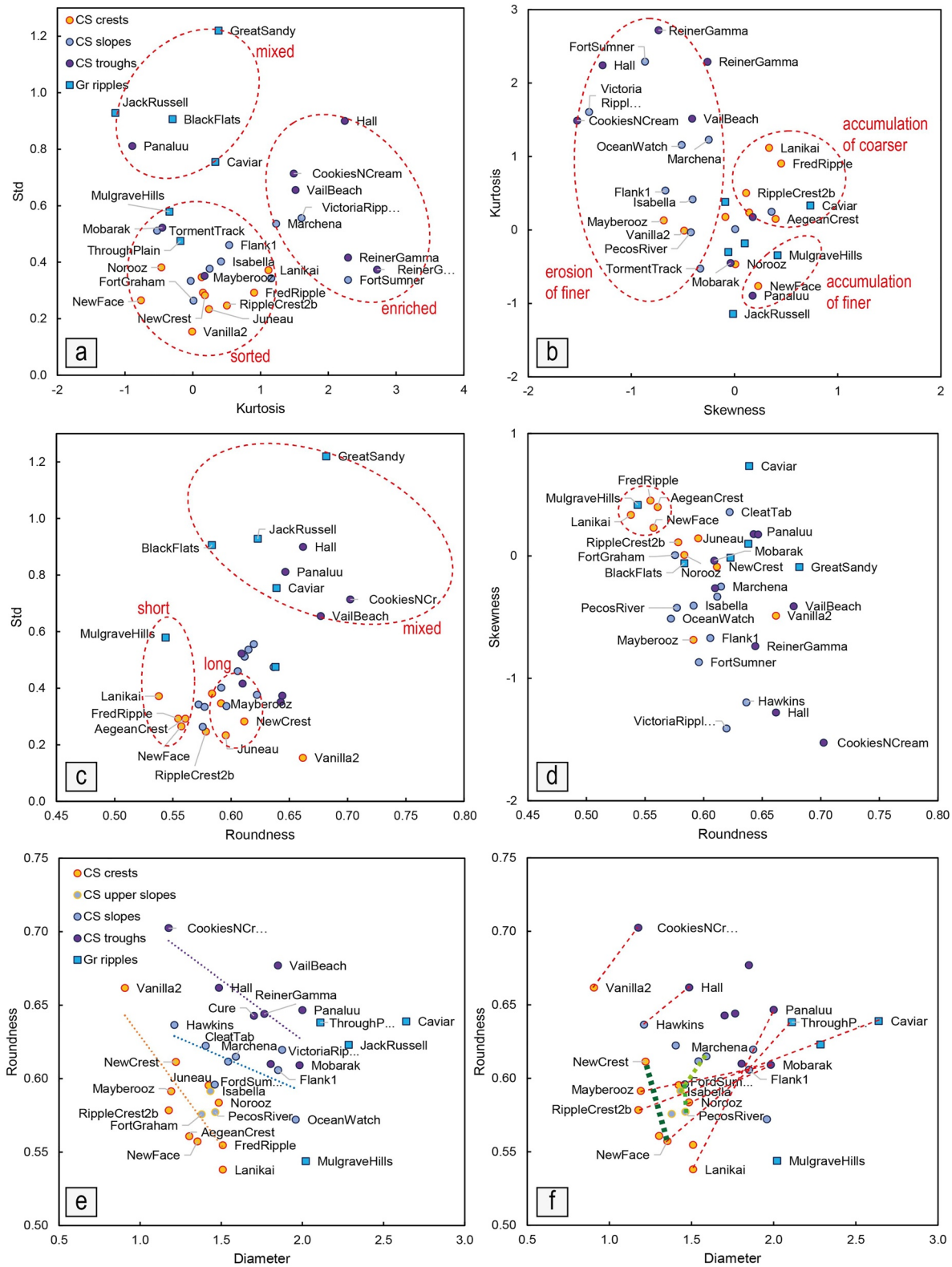

Figure 13. Analyses of very coarse sand and gravel from coarse-grained ripples: (a), Standard deviation (std, mm) versus kurtosis (phi), (b) kurtosis (phi) versus skewness (phi), (c) standard deviation (mm) versus roundness, (d) skewness (phi) versus roundness, (e) mean diameter (mm) versus roundness, (f) roundness versus mean diameter (mm). Dashed lines indicate samples from different parts of the same ripple: red—between crest/slope and slope/trough; light green—between upper and lower slope; dark green—between surface and subsurface layers. Ovals—description in the text.

slope. The grains in the subsurface layer are more rounded than on the surface. The least rounded grains are in the ripple crest characterized by good sorting (Figure 13c) and positive skewness (Figure 13d).

3.8. Chemical Composition of APXS Sediment Groups

The following APXS sediment groups were distinguished on the basis of visual inspection of MI images for a given APXS target (Table S1 and Figure S7 in Supporting Information S1): A—gravel co-occurring with various sands; B—coarse, fine, and very find sands; C—fine sands mixed with very fine sands; D—very fine sands mixed with dust; E—mixed grain fraction, and grains on bedrock, boulders. It should be noted that dust is present to some extent in all APXS sediment groups. However, due to the limited resolution of the MI images, it is not possible to establish the exact amount of dust in the studied targets. Visual inspection of the PANCAM and MI images only indicated that dust, which is pinkish and more cohesive than other fractions, is present especially in group D.

3.8.1. Group A

Within the gravel-sand group two distinct clusters are visible in Si, Al, Fe, and Mg content. Clusters are only weakly visible with respect to S and Ca (Figure 14). The clusters refer to Endeavour crater and the plains (Figure 14) and correspond to non-spherule and spherule rich targets respectively. The samples from the crater are enriched in Si, Al, Mg, and Ca compared with the plain sediments. The plain sediments within this group are relatively enriched in Fe (Figure 14). In the case of gravels, we observe a bimodal distribution in Fe abundance with one maximum similar to that observed in fine sands and dust and the second one at about 30 wt.% (Figure 15).

3.8.2. Group B

The very coarse to very fine sands were studied only on the plains. The element concentrations for this group are very similar to the samples from the plains in group A (Figures 14 and 15). There are also visible positive and negative correlations regarding Si versus Al and Fe versus Mg (Figure 14).

3.8.3. Group C

The fine to very fine sands are enriched in Si, Al, Mg, and Ca, making them quite similar to the Endeavour locations in class A, dominated by gravel. There was no clearly visible compositional difference between the plains and Endeavour crater in group C (Figure 14). The median concentration of FeO was 18 wt.% (Figure 15).

3.8.4. Group D

The very fine sands and dust display a composition similar to that of group C with respect to Si, Al, Fe, and Mg. However, both on the plains and at Endeavour crater, these sediments are enriched in sulfur compared to other groups (Figure 14). FeO shows a very uniform and normal distribution for the smallest fractions with a median value of 18.33 wt.%. SO_3 content is clearly increased in this group, with a median of 7.34 wt.% (Figure 15).

3.8.5. Group E

Sediments within this group have various chemical compositions. However, similar to group A, two clusters may be distinguished here. The concentrations of Si and Al are very similar to those of group A within Endeavour crater (Figure 14). The distribution of SO_3 seems to be bimodal; however, it is flattened with a median of 6.50 wt.% (Figure 15).

The determination of the normative mineral composition using the CIPW algorithm allowed us to classify most samples as basalt/andesite on the QAPF (quartz-alkali feldspar-plagioclase-feldspathoid) diagram for the volcanic rock classification (Le Maitre et al., 2002; Figure 16). "Juneau" has the most silica-depleted composition, which is in the tephrite field. Four samples show an elevated normative quartz content ("George Drouillard," "George Drouillard 2," "Esperance" and "Haiwassee").

3.9. Density Estimation

The results of the grain density estimation based on the CIPW normative composition are shown in Figure 17. The estimations assume no porosity in grains. With sedimentary material, it is reasonable to take only microporosity into account, and the contribution of this is small, below 5% (Saar & Manga, 1999). Spherules and fragments of spherules do not show evidence of porosity on the scale of the MI images (Figures 3h and 3l).

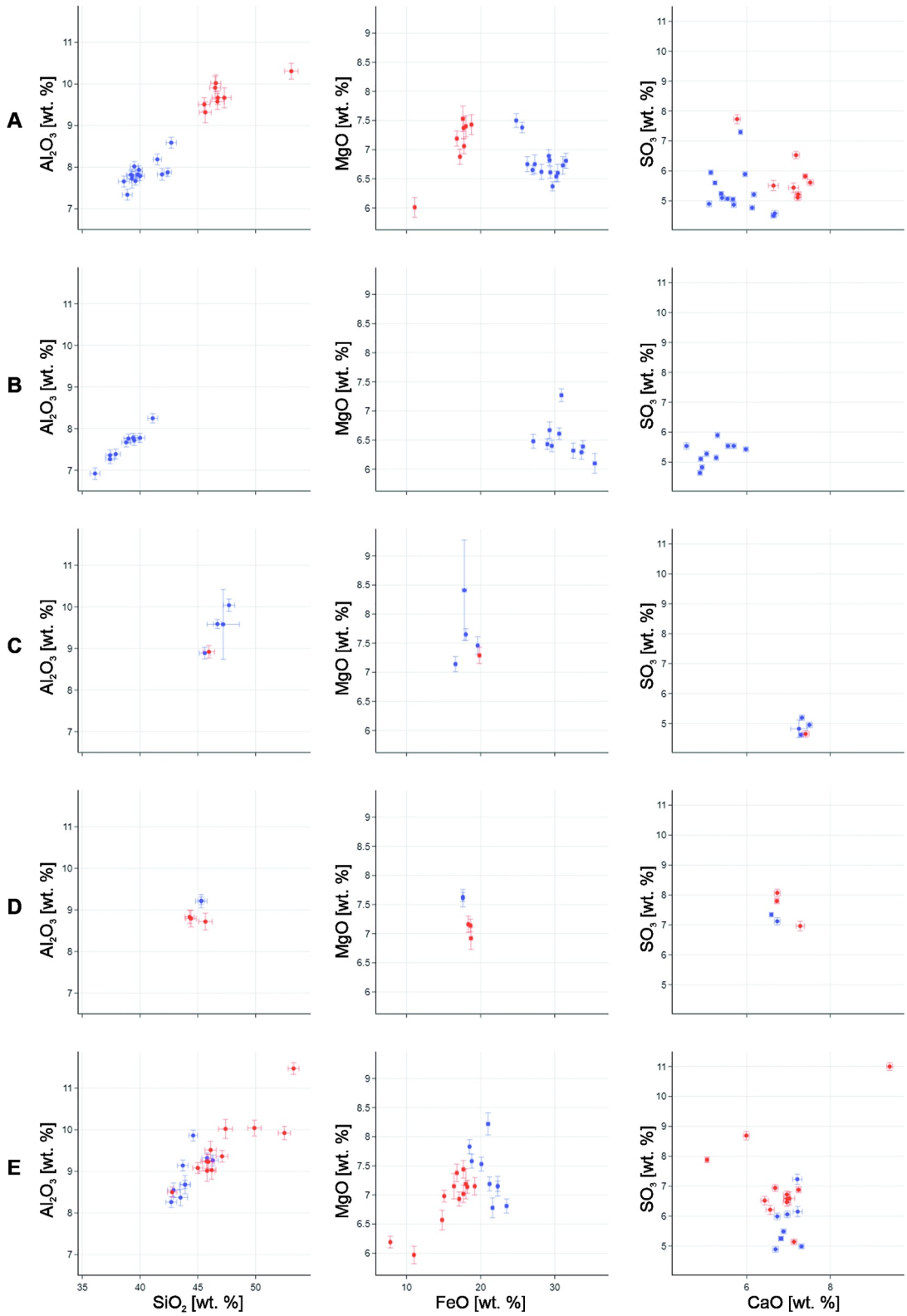

Figure 14. APSX oxides abundance plots with error bars: for APXS sediment groups denoted by letters A–E (see Section 3.8). Red dots—targets at the Endeavour crater rim, blue dots—targets on the plains.

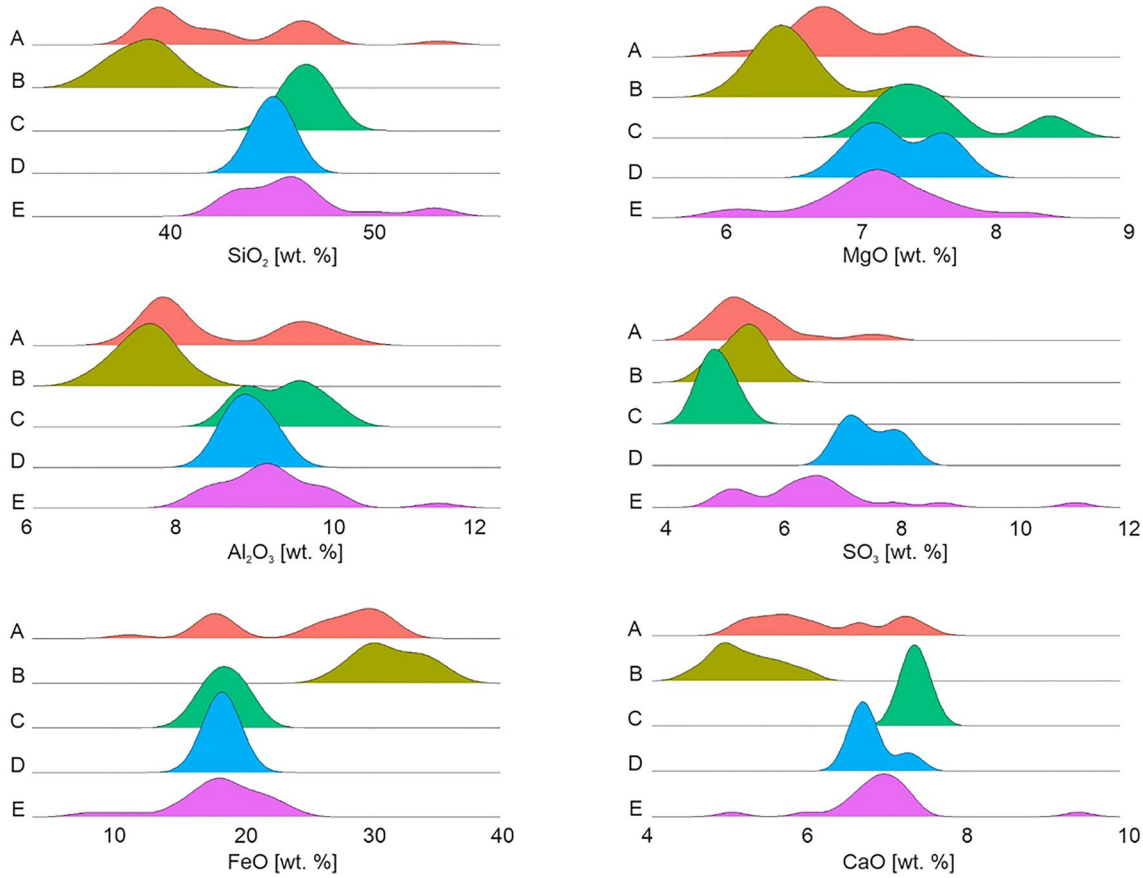

Figure 15. Simplified density plots (ridgeplots) for SiO_2, Al_2O_3, FeO, MgO, SO_3, and CaO for APXS sediment groups denoted by letters A–E (see Section 3.8).

The densities are between 2,907 and 3,570 kg/m^3. In general, coarse sands show the highest results, with maximum values for the targets from coarse-grained ripples on the plains and well-sorted coarse sands in bedrock fractures. High values (approximately 3,400–3,500 kg/m^3) were observed for the plains-related gravels and lower (approximately 2,900–3,100 kg/m^3) for the Endeavour crater gravels. All three other classes have densities of about 3,000–3,100 kg/m^3 with some anomalously low values in "Esperance" and "George Drouillard" (approximately 2,900 kg/m^3). The results are strictly related to the QAPF classification (Figure 16) as they are derived from the same data.

4. Discussion and Conclusions

4.1. Regional and Local Sand Variations

Based on the results, two sand units were distinguished: the plains unit and the Endeavour crater unit. In terms of grain size, the only difference between these two units is in coarse-grained ripple samples. Large grains such as those in the "MulgraveHills" ripple at the Endeavour crater rim were not found on the plains, although many samples from coarse-grained ripples on the plains were studied. There is also a distinct regional difference in the shape of very coarse sand and gravel grains. On the plains, due to the presence of spherules, very coarse sand and gravel grains are much more rounded than grains at the Endeavour crater rim. A parameter that distinguishes spherules from other grains is their roundness and not their circularity or aspect ratio, as spherules are not necessarily spherical (Figure 3h). The fine sands do not indicate any regional differences between the plains and the Endeavour crater rim.

The samples from the coarse-grained ripple crests are different from all the other samples. They are composed of the smallest, the best sorted, and the least rounded grains as compared to other settings, such as gravel-sand sheets. The fine sands in fine sand ripples, on the other hand, are very similar to fine sands in sand shadows, and other settings, with one exception—grains deposited on bedrock and boulders.

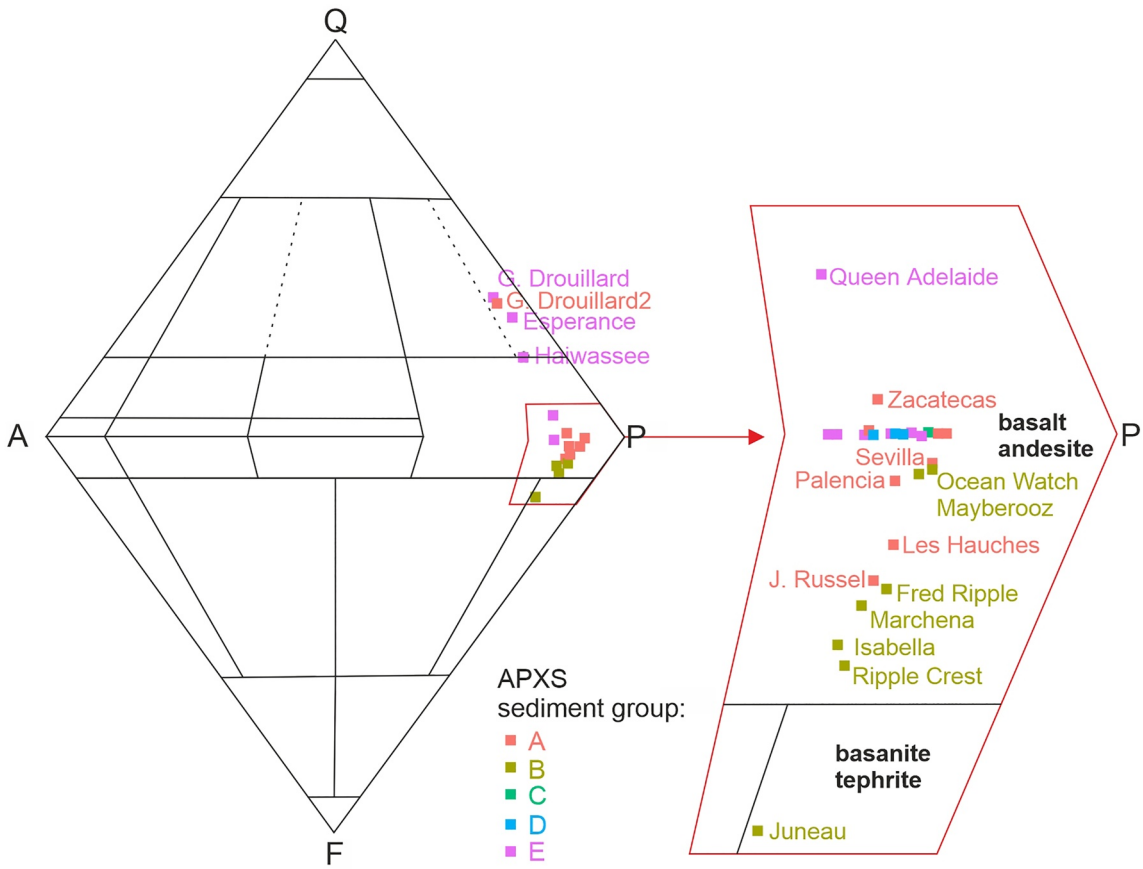

Figure 16. Volcanic rock classification diagram in the QAPF system for APXS analyzed targets. Letters A–E denote sediment groups described in Section 3.8.

Regarding the chemical composition, there is a clear difference between gravel found on the plains and at the rim of Endeavour crater, expressed mainly by FeO content. In addition, on the plains, very coarse sands have FeO content similar to that of gravel. The existence of these two geochemical units is related to the presence of hematite-rich spherules on the plains, which are absent at the Endeavour rim. Dust and very fine sands are homogeneous and enriched in SO_3 compared to other fractions. Fine sands are also homogeneous along the traverse.

There is also a local variation in the material on the plains. Iron-rich material is concentrated on the ripple crests (e.g., "Ripple Crest") and within lag deposits in bedrock fractures composed of well-sorted coarse sands ("Alamagordo Creek"). The more basanite composition of the ripple-crest-related targets in the CIPW normative calculation is most likely the consequence of the enrichment of this material in FeO in the form of hematite.

The chemical composition of MP fine sands is similar to sediments from other Martian locations analyzed by APXS (Figure 18; see also O'Connell-Cooper et al., 2017). However, coarse sand and gravel on the MP plains is characterized by higher FeO content as compared to other sediments investigated by APXS on Mars, and this is likely due to the prevalence of hematite spherules on MP (Figure 18).

4.2. Sources and Shaping Processes

The source of gravel is mostly local, as shown by the differences in the chemical compositions between the plains and the Endeavour crater rim. The gravel at the rim of Endeavour crater can be produced from the disintegration of Matijevic formation rocks. The Matijevic formation is pre-Endeavour, light-toned (sometimes with dark coating), fine-grained sedimentary rock with basaltic composition in the TAS (total alkali vs. silica) classification, containing on average 16 wt.% of FeO and 48.8 wt.% of SiO_2 (Bouchard & Jolliff, 2018; Mittlefehldt et al., 2021). These rocks are comparable to the gravels from Endeavour crater (see red dots in Figure 14 on the FeO-MgO diagram for group A).

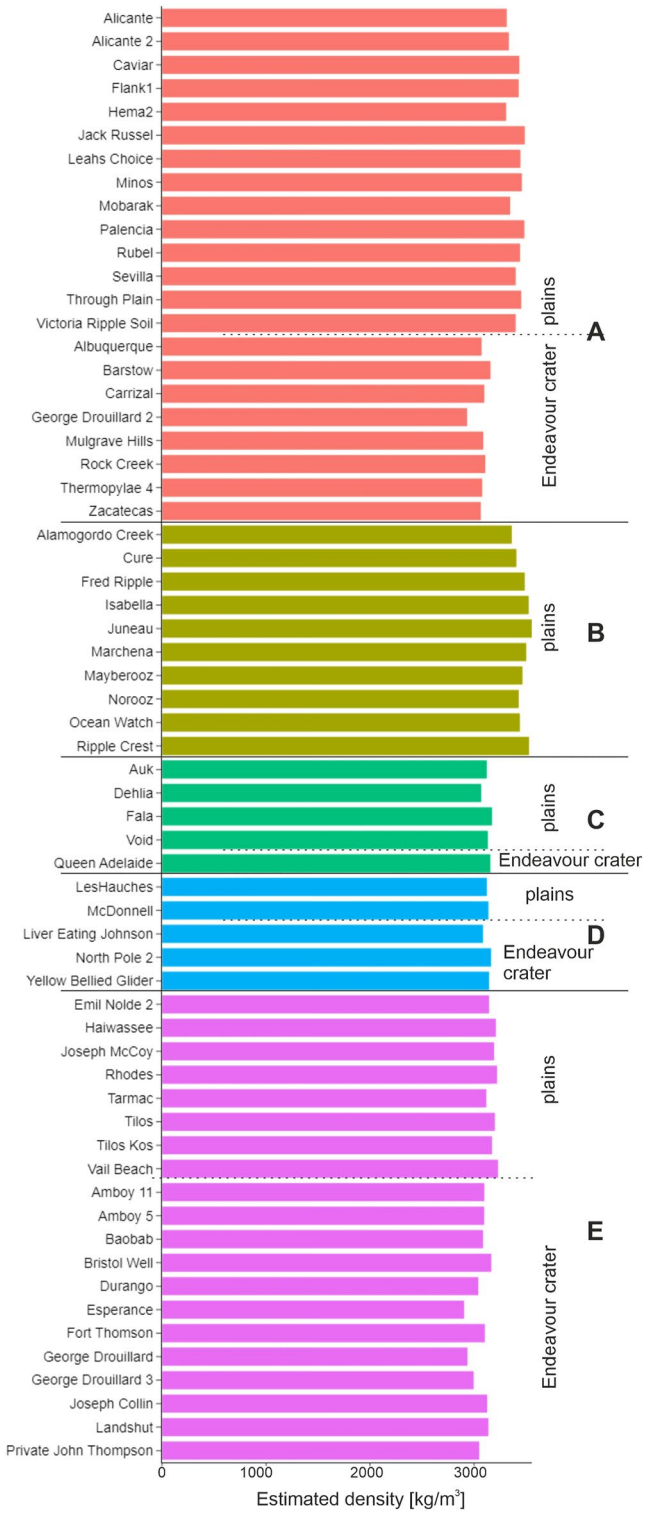

Figure 17. Density estimation for APXS targets by location and APXS sediment groups denoted by letters A–E and described in Section 3.8.

The geochemical results indicate that on the plains, coarse sands and spherules are similar in composition. Therefore, the coarse sand on the plains has its origin partially in spherules, and partially in other gravel grains, the source of which is related to rocks brought to MP via the ejection of rock fragments during impact cratering that took place outside MP (Squyres et al., 2006). The spherules are found primarily in the gravel fraction, but they erode into angular coarse sand grains (Figure 3l). These angular coarse sand grains have lower roundness than the spherules and can be transported by wind and over time become more rounded. However, the roundness of the transported coarse sand grains is still lower than the roundness of the spherules. The high roundness of the spherules is related to their genesis not to their transport path lengths. Therefore, on the plains, the most rounded are gravel grains (spherules) not coarse sand grains.

The dark fine sand on the plains and at the Endeavour crater rim is probably produced by erosion of layers inside craters (Tirsch et al., 2011), as well as from disintegration of basaltic rocks and gravel, which were brought to MP via impact cratering (Squyres et al., 2006). As fine sands can be transported in saltation over long distances, it is also possible that the studied dark fine sands have an origin outside of MP. The bright fine sand is produced from the erosion of the Burns formation rock matrix (Figure 4j). As this rock matrix is very susceptible to physical erosion, the sediments produced from these rocks may spend a relatively short time in a fine sand form and disintegrate into very fine sand and dust.

Dust is transported in global dust storms; therefore, it is expected to be well mixed and uniform across the planet. Dust on MP is similar to dust investigated previously in other locations (Beger et al., 2016). Sediments with dust on MP are enriched in SO_3. This may be related to the presence of jarosite in very fine sand and dust fractions. The presence of jarosite was confirmed on MP by Mössbauer analyses at the early stage of the Opportunity mission (Klingelhöfer et al., 2004). Therefore, Burns formation rocks containing jarosite may be a source of dust. Hence, the source of dust on MP can be global and local at the same time.

4.3. Aeolian Sediment Transport Constraints

Along the traverse, aggregates composed of very fine particles (below the MI resolution) related to bright dust wind streaks are often accompanied by bright small ripples (Figure 4c). As ripples are formed by grains that are transported in saltation or reptation, these sediments cannot be made up of individual dust grains, which are transported by suspension. Hence, these bedforms must be composed of very fine sand particles or of aggregates made up of dust and very fine sand grains. Bright wind streaks and bright small ripples are active on MP (Figure 19, see also Sullivan et al., 2005). The presence of fine sand grains on the magnets, located on the rover deck (Figure S2c in Supporting Information S1), indicates that these grains are easily transported by wind. Changes in sand shadows and wind streaks composed of fine sand grains were also observed on MP (Chojnacki et al., 2015; Geissler et al., 2008). Very coarse sand grains were observed to be transported by wind at the Endeavour crater rim (Chojnacki et al., 2015), mainly in places where deposits were previously disturbed by the rover wheels. Crests of large (m-scale wavelength) coarse-grained ripples on the plains are oriented N-S, but crests of small (dm-scale wavelength) coarse-grained ripples, more susceptible to changes, are oriented to the NNE-SSW direction (Fenton et al., 2018; Sullivan et al., 2005) by modern NW winds (Chojnacki et al., 2011;

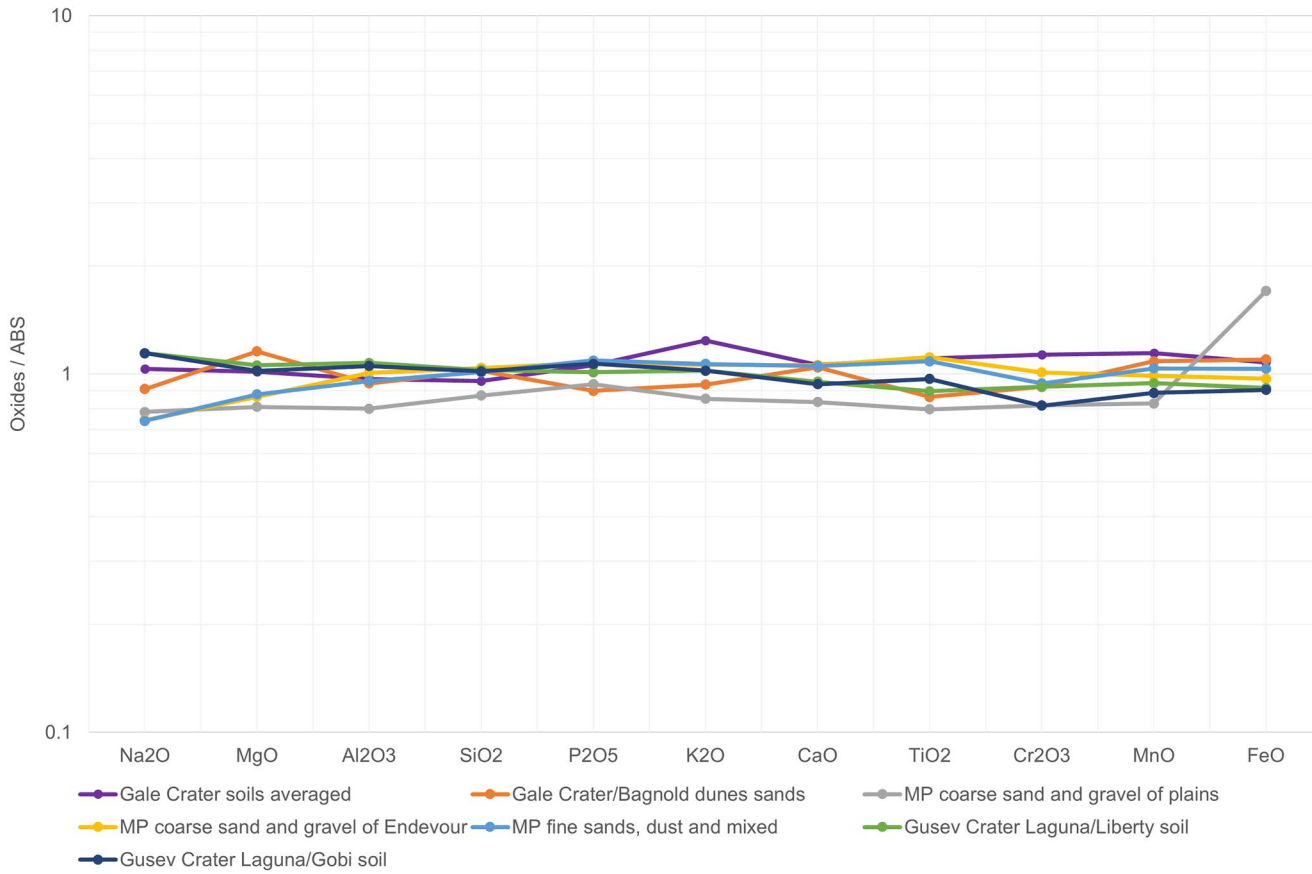

Figure 18. Major oxides renormalized to volatile free (i.e., SO_3 and Cl free) rationed to the Martian average basaltic soil (ABS) after O'Connell-Cooper (2017). Gale crater average soils and Bagnold dunes sands average compositions after O'Connell-Cooper (2017) and Gusev crater soils after Ming et al. (2008).

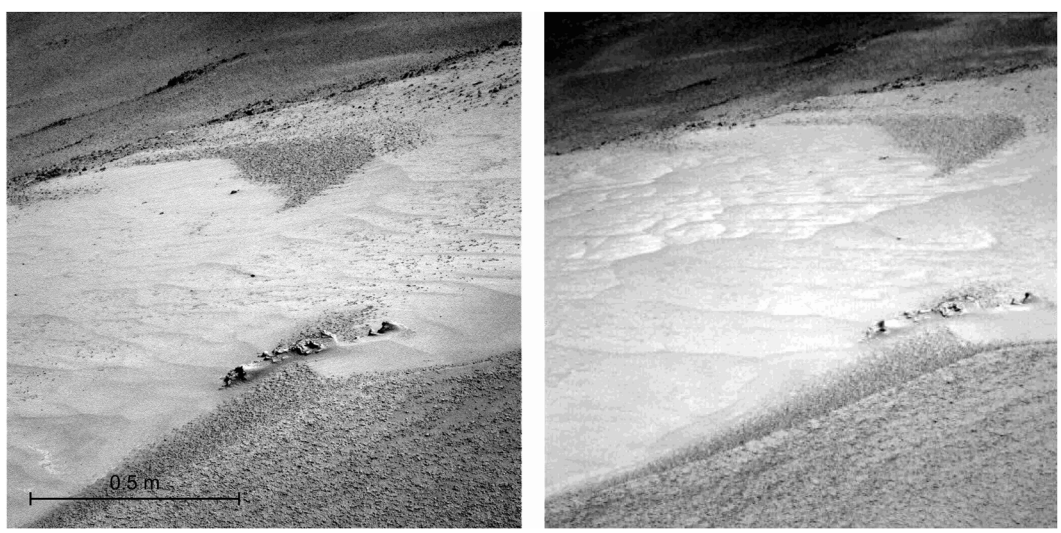

Figure 19. Small changes in a field of bright small ripples between sol 2804 (left image), and sol 2914 (right image). Both images from PANCAM. South is toward the top. Scale bar is representative of the central part of the images.

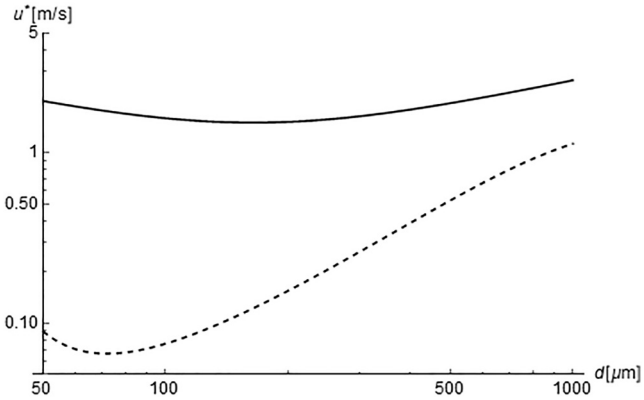

Figure 20. Fluid (solid line) and impact (dashed line) threshold shear velocities versus particle size for Mars for basaltic grains with density 3,000 kg/m^3.

Fenton et al., 2015). This observation indicates that coarse sand grains in the coarse-grained ripples' armoring layers are transported by wind on MP.

The shear velocity of wind necessary to initiate the motion of grains from a bed is called the fluid threshold shear velocity (u*ft) (Bagnold, 1941). For Mars, this value can be calculated from the expression by Shao and Lu (2000) used previously by Jerolmack et al. (2006), which is derived from Iversen and White (1982). The impact threshold shear velocity (u*it) on Mars is much lower and can be calculated from the expression of Kok (2010). Aeolian transport occurs only when these threshold values are met (Figure 20).

On MP, fine sand grains in deposits that were formed by aeolian processes, such as sand shadows or fine sand ripples, have typical diameters of around 100 and 130 μm. The former value is very close to the minimal value of the impact shear velocity threshold (around 70 μm, Figure 20). We cannot determine whether smaller grains with diameters closer to the impact threshold value are more common in bedforms due to the MI image resolution limit. The latter value (130 μm) is close to the minimum of the fluid shear velocity threshold.

The minimum fluid shear velocity to initiate the saltation of fine sand on MP is 1.5 m/s, and to sustain this saltation is 0.06 m/s. These conditions must be easily met considering the activity of bedforms and individual particles observed on MP. The slightly different skewness and kurtosis of fine sands deposited on bedrock and boulders in comparison to grains in other settings (Figure 10) can be related to recent wind events, which were responsible for the mixing, deflating, and sorting of these grains.

For very coarse sands, we focus only on the fluid threshold, as the impact threshold expression is only valid for grains smaller than 1 mm. On the plains, the median and mean diameter for very coarse sand on coarse-grained ripple crests is close to 1.3 mm. This value is similar to that of Jerolmack et al. (2006), which was found early in the Opportunity rover mission. Our estimate of very coarse sand grain density is 3,500 kg/m^3 without microporosity and 3,300 kg/m^3 including 5% microporosity. These values are lower than the previous estimates (4,100 kg/m^3, Jerolmack et al., 2006; Sullivan et al., 2005). The very coarse sand grains are also highly circular (average 0.87); therefore, their shape should not influence the threshold values. For such parameters, the fluid threshold shear velocity is 3.2 m/s. The impact threshold shear velocity is probably much lower. The grains in the coarse-grained ripple armor are not transported by saltation. Therefore, the shear velocity must be slightly lower but close to 3.2 m/s (Jerolmack et al., 2006). At the Endeavour crater rim, there are ripples armored by still coarser grains, with the median and mean diameters of 2 mm ("Mulgrave Hills") and a density of around 3,100 kg/m^3. For such grains, the fluid threshold shear velocity ranges from 3.7 m/s (including microporosity) to 3.8 m/s (without microporosity). These are much larger values than those on the plains. In addition, MulgraveHills sample grains have lower roundness (Figure 13f), indicating that their transport paths were not very long. It can be inferred that strong episodic wind events must occur at the Endeavour crater rim, but do not occur on the plains. Probably they are induced by the crater topography.

Along the traverse of the Opportunity rover, two types of bedforms were observed: bedforms entirely composed of fine sand (wind streaks, fine sand ripples, sand shadows), and bedforms composed mainly of fine sand but entirely covered by coarse-grained armor (coarse-grained ripples). On MP, fine sand bedforms are mainly composed of grains <0.15 mm, similar to fine sand bedforms in Gale crater (Weitz et al., 2018, 2022). The very coarse sands in armoring layer of coarse-grained ripples on MP are very similar to sands observed on the coarse-grained ripples in Gusev and Gale craters (1–2 mm in diameter, Cabrol et al., 2014; Weitz et al., 2022). However, in Gale crater, coarse-grained ripples composed of still larger gravel grains than in the "Mulgrave Hill" ripple were observed (Sullivan et al., 2022; Weitz et al., 2022). Bedforms composed of medium sands (0.2–0.5 mm grains) were found in Gale and Gusev craters (Cabrol et al., 2014; Weitz et al., 2018, 2022), but they are not present on MP.

The most important question is why there are no medium sands (0.25–0.50 mm) along the Opportunity traverse, while they are very common in Gale crater (Gough et al., 2021; Weitz et al., 2018, 2022) and Gusev crater (Cabrol et al., 2014). This difference may be related to the character of the sand sources. However, medium sands do not appear either on the plains or at the Endeavour crater rim, and these two locations are different from a geological point of view. It is also quite hard to believe that basaltic rock fragments do not disintegrate into medium-sand

particles. Although several individual medium sand grains were found around Victoria crater and at the Endeavour crater rim (Figures 7 and 9; Table S2 in Supporting Information S1), they were mainly present only in one place along the Opportunity rover traverse—inside Endurance crater (Figure 7; Table S2 in Supporting Information S1). It was unfortunately the only relatively large crater interior investigated by the rover.

Medium sands are often found on Mars in dunes and ripples (Cabrol et al., 2014; Gough et al., 2021; Weitz et al., 2018, 2022); therefore, they are transported in saltation. Dunes, which on MP are located only in some of the largest craters, were observed to change their shape and position (Chojnacki et al., 2011). The sand in these dunes was not measured directly because they are very far from the rover traverse, but it is known that in other places on Mars, sand dunes are composed of fine and medium sand particles (>0.2 mm, see e.g., Weitz et al., 2018).

The fluid and impact threshold shear velocity for 0.3 mm grains, assuming that they are basaltic in composition, are 1.6 and 0.3 m/s, respectively (Figure 20). These values should be met on MP easily as they are not very far from the values obtained for the fine sands, and much lower than those obtained for the very coarse sands.

A reasonable hypothesis is that medium sand grains were more common on the plains in the past than today; however, due to the slow weathering, the lack of source material, and the strong deflation, they were mostly trapped in relatively larger craters, from which they cannot be blown away unlike finer sands. In craters, they formed dunes and were probably trapped inside transverse aeolian ridges (TARs) and coarse-grained ripples.

Another important question is whether fine sand grains (0.13 mm) can move 10 times their size very coarse sand particles (1.3 mm), which would be necessary to form coarse-grained ripples that are so common on the plains. Bagnold (1941) observed that grains in saltation can move grains up to 6 times their size. The more recent work by Tholen et al. (2022) on the formation of bedforms composed of bimodal (finer and coarser) sands, as is often the case for coarse-grained ripples, predicts that on Mars the maximum size of the coarser fraction should be 4.5 times size of the maximum size of the fraction transported in saltation. This would require that the saltating grains on MP were larger than 0.22 mm—mainly in the medium sand fraction—the fraction that is missing on the plains. However, on Mars, this relationship between the grains in coarse-grained ripples has not been tested and further studies are necessary. Furthermore, even if we did not find medium sand grains within coarse-grained ripples it does not necessarily indicate that medium sands were not present during the ripples' formation and are not present within the ripples' interiors, which are still poorly investigated as images of only few ripple interiors were available for qualitative study.

Grains on coarse-grained ripple crests are smaller than grains on ripple slopes, which in turn are smaller than grains in ripple troughs (Figure 13f). This sequence of grain sizes is typical for coarse-grained ripples and can be explained by the sorting of sands by wind. The most susceptible to transport grains of coarse sand are transported in a creep-like mode up to ripple crests. In ripple troughs, on the other hand, smaller particles are deflated, and gravel particles (not transported by wind) are common (Jerolmack et al., 2006). Therefore, the samples from ripple crests are characterized by positive skewness and the samples from slopes and troughs by negative skewness (Figure 13b). To sum it up, finer particles of coarse sand are removed from the slopes and troughs and deposited on the crests. The distribution of particles in coarse-grained ripples is often opposite to that in fine sand ripples. In fine sand ripples, the coarsest sand particles are on ripple crests and the finest in ripple troughs (Bagnold, 1941). Such a sequence of particle sizes was observed on fine and medium sand ripples in Gale crater (see e.g., Sullivan et al., 2022; Weitz et al., 2018).

The coarse-grained ripples are well armored by coarse sand (1–2 mm), and this armoring layer protects fine sand (<0.15 mm) grains inside the ripples from deflation. Due to this induration, coarse-grained ripples are dormant. When this armor is even partially destroyed, fine particles can be removed by wind from the ripple interior. Such events may lead to a short-lived ripple activity. The last migration of coarse-grained ripples on MP dates to tens or hundreds of thousands of years ago (Fenton et al., 2015; Golombek et al., 2010). Even if the ripples are currently inactive, they are susceptible to reshaping and changes in orientation by current winds (Fenton et al., 2018; Sullivan et al., 2005). Our results confirm this observation, as the largest positive skewness was found for the crests of all smaller coarse-grained ripples ("FredRipple," "AegeanCrest," "Lanikai," "MulgraveHills") but one ("Vanilla2," Figure 13d).

The activity of coarse-grained ripples depends not only on the wind strength but also on the supply of saltating grains (fine and medium sands), as coarse sand grains are mobilized by the impacts of saltating particles. A

rapid increase in saltating particles can activate even inactive bedforms (Silvestro et al., 2020). At present, there is a small amount of fine and medium sand on the surface of MP. Fine sands are only present on crater floors. In other places, gravel-sand sheets with depleted fine sand fractions dominate. Therefore, currently, as the amount of fine and medium sand available for transport on MP is small, very coarse sand grains are expected to be transported over much shorter distances than in the past when coarse-grained ripples were formed and migrated. On the other hand, some changes in the orientation of coarse-grained ripples are observed (Fenton et al., 2018; Sullivan et al., 2005), and therefore, erosion and accumulation of coarse sands in ripples must occur on MP. Our results confirmed these expectations and observations. There is a negative correlation between roundness and skewness in the case of coarse-grained ripple samples (Figure 13d), which indicates that locations in which coarse sand grains accumulate are characterized by lower roundness. Lower roundness implies shorter transport path lengths. The least rounded grains are on the ripple crests characterized by good sorting (Figure 13c) and positive skewness (Figure 13d), indicating that these grains were transported and accumulated. This is an unexpected result, as grains transported by wind should be more rounded than grains close to a source. In addition, the grains on the crests are less rounded than the grains on the slopes (which are larger than the grains on the crests) and the grains in the subsurface layers of coarse-grained ripples (which are smaller than the grains on the crests, Figure 13f). This cannot be explained by the presence of spherules, as spherules are typically not present in the coarse sand fraction. Also, grains on the ripple crests were transported more recently than grains in the subsurface layers or grains in locations where sediments are not well sorted and characterized by negative skewness (slopes and troughs), as in such places, coarser grains, less susceptible to transport, are more common. Therefore, even now relatively freshly fragmented spherules (Figure 3l) or granules in the form of coarse sand grains can accumulate on ripple crests. For these relatively young sand grains, the transport path length is much shorter than that of older grains, transported in previous epochs. This can explain the observation that coarse sand grains currently mobilized by the wind and accumulated on ripple crests have lower roundness than coarse sand grains trapped in the coarse-grained ripple interiors, troughs, and slopes.

4.4. Conclusions

Sediments composed of very coarse sand and gravel are different on the plains and at the rim of Endeavour crater. On the plains, they are characterized by more rounded grains and are enriched in iron in comparison to the sediments at the crater rim. The source of these grains is local, and on the plains, originates in the hematite spherules.

Fine sand and dust sediments are similar across the studied area. Unconsolidated sediments on MP are in general similar to unconsolidated sediments observed in other locations on Mars, except for gravel fractions on the MP plains, which are enriched in FeO due to the presence of hematite spherules.

The sands along the Opportunity traverse are depleted in grains larger than 0.2 mm and smaller than 1 mm (Figure 2). These grains have apparently been removed from the plains and trapped in depressions, such as relatively large craters (larger than about 100 m), from which they cannot be blown away as easily as fine sand. In the largest craters on MP (>5 km in diameter), these medium sands form dunes. Other bedforms, such as large (>50 cm tall) ripple-like features that can be large coarse-grained ripples or small TARs, are also found in larger craters (>90 m in diameter), and it is possible that medium sands are trapped under the armor of those bedforms.

Coarse-grained ripples on the plains are currently not migrating, but they can still be prone to reshaping and changes in orientation due to current winds. Our results confirm this low activity as the transport path lengths of currently transported coarse sand grains are expected to be shorter than the transport paths of grains carried by the wind in the past epochs when coarse-grained ripples migrated.

The following sequence of processes may be responsible for shaping the studied deposits:

1. On the plains, the erosion of Burns formation rocks derives hematite spherules that are more resistant to physical erosion and produce fine sand and dust enriched in sulfur. The partition of spherules and mixing them with other types of particles produce coarse sands.
2. At the Endeavour crater rim, aeolian processes and mass transport of impact-generated rocks lead to the production of gravel, coarse, and fine sands.
3. Long-distance transport of dust and fine sands results in their homogenization on MP. Short-distance transport of coarse sands and gravels does not allow mixing of these deposits, leading to differences in the composition and shape of coarse sands and gravels between the plains and the Endeavour crater rim.

4. On the plains, the accumulation of fine and coarse sands by aeolian processes favors the formation of coarse-grained ripples, whereas higher deflation and lower deposition rates of fine and medium sands not protected by armoring layers of coarse sand grains produce lag deposits. Medium sand accumulates in relatively larger craters of MP, where they can form dunes and can be trapped within coarse-grained ripples and TARs.

Conflict of Interest

The authors declare no conflicts of interest relevant to this study.

Data Availability Statement

Opportunity's data used in this study are publicly available via the NASA Geosciences Node of the Planetary Data System (https://pds-geosciences.wustl.edu/missions/mer/geo_mer_datasets.htm) and can be accessed through the MER Analyst's Notebook at https://an.rsl.wustl.edu/mer/. MI data (Maki, 2004c), PANCAM data (Bell, 2004), NAVCAM data (Bell, 2009), NAVCAM mosaics (Maki, 2004a). HAZCAM data (Maki, 2004b), APXS data (Gellert, 2019). Overlying and mosaicking of MI images were done using Adobe Photoshop. For detection and measurement of particles in images we used the PADM algorithm (Kozakiewicz, 2018) implemented in Wolfram Mathematica (Kozakiewicz, 2023) and for roundness calculations we used the algorithm by Zheng and Hryciw (2016) implemented in the MathWorks MATLAB by Zheng (2023; https://www.mathworks.com/matlabcentral/fileexchange/60651-particle-roundness-and-sphericity-computation). Full-resolution Figure S7 in Supporting Information S1, all tables, also including a table with APXS data for all targets studied in this work, are archived at Kozakiewicz (2023).

Acknowledgments
The work was funded by the Anthropocene Priority Research Area budget under the program "Excellence Initiative—Research University" at the Jagiellonian University. The authors thank Ken Herkenhoff and a second, anonymous reviewer for their helpful comments on this paper.

References

Arvidson, R. E., Ashley, J. W., Bell, J. F., III., Chojnacki, M., Cohen, J., Economou, T. E., et al. (2011). Opportunity Mars Rover mission: Overview and selected results from Purgatory ripple to traverses to Endeavour crater. *Journal of Geophysical Research*, *116*, E00F15. https://doi.org/10.1029/2010JE003746

Arvidson, R. E., Bell, J. F., Bellutta, P., Cabrol, N. A., Catalano, J. G., Cohen, J., et al. (2010). Spirit Mars Rover Mission: Overview and selected results from the northern Home Plate Winter Haven to the side of Scamander crater. *Journal of Geophysical Research*, *115*, E00F03. https://doi.org/10.1029/2010JE003633

Arvidson, R. E., Squyres, S. W., Anderson, R. C., Bell, J. F., Blaney, D., Brückner, J., et al. (2006). Overview of the Spirit Mars Exploration Rover mission to Gusev crater: Landing site to Backstay Rock in the Columbia Hills. *Journal of Geophysical Research*, *111*(E2), E02S01. https://doi.org/10.1029/2005JE002499

Bagnold, R. A. (1941). *The physics of blown sand and desert dunes*. Chapman and Hall.

Bell, J. (2004). MER 1 Mars Pancam radiometrically calibrated RDR V1.0 [Dataset]. NASA Planetary Data System. https://doi.org/10.17189/1520220

Bell, J. (2009). MER 1 Mars NAVCAM 3 radiometric RDR SCI V1.0 [Dataset]. NASA Planetary Data System. https://doi.org/10.17189/1520327

Bell, J. F., III., Squyres, S. W., Herkenhoff, K. E., Maki, J. N., Arneson, H. M., Brown, D., et al. (2003). Mars exploration rover Athena panoramic camera (Pancam) investigation. *Journal of Geophysical Research*, *108*(E12), 8063. https://doi.org/10.1029/2003JE002070

Berger, J. A., Schmidt, M. E., Gellert, R., Campbell, J. L., King, P. L., Flemming, R. L., et al. (2016). A global Mars dust composition refined by the Alpha-Particle X-ray Spectrometer in Gale Crater. *Geophysical Research Letters*, *43*(1), 67–75. https://doi.org/10.1002/2015GL066675

Bouchard, M. C., & Jolliff, B. L. (2018). A systematic method for classifying and grouping Late Noachian and Early Hesperian rock targets analyzed by the Mars Exploration Rover Opportunity at Endeavour crater, Mars. *Journal of Geophysical Research: Planets*, *123*(11), 2980–3004. https://doi.org/10.1029/2018je005631

Cabrol, N. A., Herkenhoff, K., Knoll, A. H., Farmer, J., Arvidson, R., Grin, E., et al. (2014). Sands at Gusev crater, Mars. *Journal of Geophysical Research: Planets*, *119*(5), 941–967. https://doi.org/10.1002/2013JE004535

Chojnacki, M., Burr, D. M., Moersch, J. E., & Michaels, T. I. (2011). Orbital observations of contemporary dune activity in Endeavor crater, Meridiani Planum, Mars. *Journal of Geophysical Research*, *116*, E00F19. https://doi.org/10.1029/2010JE003675

Chojnacki, M., Johnson, J. R., Moersch, J. E., Fenton, L. K., Michaels, T. I., & Bell, J. F. (2015). Persistent aeolian activity at Endeavour crater, Meridiani Planum, Mars; new observations from orbit and the surface. *Icarus*, *251*, 275–290. https://doi.org/10.1016/j.icarus.2014.04.044

Fenton, L. K., Carson, H. C., & Michaels, T. I. (2018). Climate forcing of ripple migration and crest alignment in the last 400 Kyr in Meridiani Planum, Mars. *Journal of Geophysical Research: Planets*, *123*(4), 849–863. https://doi.org/10.1002/2017JE005503

Fenton, L. K., Michaels, T. I., & Chojnacki, M. (2015). Late Amazonian aeolian features, gradation, wind regimes, and sediment state in the vicinity of the Mars Exploration Rover Opportunity, Meridiani Planum, Mars. *Aeolian Research*, *16*, 75–99. https://doi.org/10.1016/j.aeolia.2014.11.004

Geissler, P., Johnson, J., Sullivan, R., Herkenhoff, K., Mittlefehldt, D., Fergason, R., et al. (2008). First in situ investigation of a dark wind streak on Mars. *Journal of Geophysical Research*, *113*(E12), E12S31. https://doi.org/10.1029/2008JE003102

Gellert, R. (2019). MER APXS derived oxide data bundle [Dataset]. NASA Planetary Data System. https://doi.org/10.17189/1518973

Golombek, M., Robinson, K., McEwen, A., Bridges, N., Ivanov, B., Tornabene, L., & Sullivan, R. (2010). Constraints on ripple migration at Meridiani Planum from Opportunity and HiRISE observations of fresh craters. *Journal of Geophysical Research*, *115*, E00F08. https://doi.org/10.1029/2010JE003628

Gough, T. R., Hugenholtz, C. H., & Barchyn, T. E. (2021). Re-evaluation of large Martian ripples in Gale crater: Granulometric evidence for an impact mechanism and terrestrial analogues. *Journal of Geophysical Research: Planets*, *126*(12), e2021JE007011. https://doi.org/10.1029/2021JE007011

Herkenhoff, K. E., Golombek, M. P., Guinness, E. A., Johnson, J. B., Kusack, A., Richter, L., et al. (2008). In-situ observations of the physical properties of the Martian surface. In J. F. Bell III (Ed.), *The Martian surface: Composition, mineralogy, and physical properties* (p. 688). Cambridge University Press.

Herkenhoff, K. E., Squyres, S. W., Arvidson, R., Bass, D. S., Bell, J. F., Bertelsen, P., et al. (2004). Evidence from Opportunity's microscopic imager for water on Meridiani Planum. *Science*, *306*(5702), 1727–1730. https://doi.org/10.1126/science.1105286

Herkenhoff, K. E., Squyres, S. W., Bell, J. F., III., Maki, J. N., Arneson, H. M., Bertelsen, P., et al. (2003). Athena microscopic imager investigation. *Journal of Geophysical Research*, *108*(E12), 8065. https://doi.org/10.1029/2003JE002076

Iversen, J. D., & White, B. R. (1982). Saltation threshold on Earth, Mars and Venus. *Sedimentology*, *29*(1), 111–119. https://doi.org/10.1111/j.1365-3091.1982.tb01713.x

Jerolmack, D., Mohrig, D., Grotzinger, J., Fike, D., & Watters, W. (2006). Spatial grain size sorting in eolian ripples and estimation of wind conditions on planetary surfaces: Application to Meridiani Planum, Mars. *Journal of Geophysical Research*, *111*(E12), E12S02. https://doi.org/10.1029/2005JE002544

Karunatillake, S., McLennan, S., & Herkenhoff, K. E. (2010). Regional and grain size influences on the geochemistry of soil at Gusev crater, Mars. *Journal of Geophysical Research*, *115*, E00F04. https://doi.org/10.1029/2010JE003637

Klingelhöfer, G., Morris, R., Bernhardt, B., Schröder, C., Rodionov, D., De Souza, P., et al. (2004). Jarosite and hematite at Meridiani Planum from Opportunity's Mossbauer spectrometer. *Science*, *306*, 1740–1745. https://doi.org/10.1126/science.1104653

Kok, J. (2010). An improved parameterization of wind-blown sand flux on Mars that includes the effect of hysteresis. *Geophysical Research Letters*, *37*(12), L12202. https://doi.org/10.1029/2010GL043646

Kozakiewicz, J. (2018). Image analysis algorithm for detection and measurement of Martian sand grains. *Earth Science Informatics*, *11*(2), 257–272. https://doi.org/10.1007/s12145-018-0333-y

Kozakiewicz, J. (2023). Sands on Meridiani Planum, Mars. *Archive_Sub*. https://doi.org/10.5281/zenodo.8309724

Krumbein, W. C. (1941). Measurement and geological significance of shape and roundness of sedimentary particles. *Journal of Sedimentary Research*, *11*(2), 64–72. https://doi.org/10.1306/D42690F3-2B26-11D7-8648000102C1865D

Le Maitre, R. W., Streckeisen, A., Zanettin, B., Le Bas, M. J., Bonin, B., Bateman, P., et al. (2002). *Igneous rocks: A classification and glossary of terms: Recommendations of the international union of geological sciences, subcommission on the systematics of igneous rocks* (p. 236). Cambridge University Press.

Madsen, M. B., Bertelsen, P., Goetz, W., Binau, C. S., Olsen, M., Folkmann, F., et al. (2003). Magnetic properties experiments on the Mars Exploration Rover mission. *Journal of Geophysical Research*, *108*(E12), 8069. https://doi.org/10.1029/2002JE002029

Maki, J. N. (2004a). MER 1 Mars navigation camera Mosaics RDR OPS V1.0 [Dataset]. NASA Planetary Data System. https://doi.org/10.17189/1520257

Maki, J. N. (2004b). MER 1 Mars hazard avoid camera linearized RDR OPS V1.0 [Dataset]. NASA Planetary Data System. https://doi.org/10.17189/1520235

Maki, J. N. (2004c). MER 1 Mars microscopic imager radiometric RDR OPS V1.0 [Dataset]. NASA Planetary Data System. https://doi.org/10.17189/1520416

Maki, J. N., Bell, J. F., III., Herkenhoff, K. E., Squyres, S. W., Kiely, A., Klimesh, M., et al. (2003). Mars exploration rover engineering cameras. *Journal of Geophysical Research*, *108*(E12), 8071. https://doi.org/10.1029/2003JE002077

McGlynn, I. O., Fedo, C. M., & McSween, H. Y. (2011). Origin of basaltic soils at Gusev crater, Mars, by aeolian modification of impact-generated sediment. *Journal of Geophysical Research*, *116*, E00F22. https://doi.org/10.1029/2010JE003712

Ming, D. W., Gellert, R., Morris, R. V., Arvidson, R. E., Brückner, J., Clark, B. C., et al. (2008). Geochemical properties of rocks and soils in Gusev crater, Mars: Results of the alpha particle X-ray spectrometer from Cumberland Ridge to home plate. *Journal of Geophysical Research*, *113*(E12), E12S39. https://doi.org/10.1029/2008je003195

Mittlefehldt, D. W., Gellert, R., van Bommel, S., Arvidson, R. E., Ashley, J. W., Clark, B. C., et al. (2021). Geology and geochemistry of Noachian bedrock and alteration events, Meridiani Planum, Mars: MER Opportunity observations. *Journal of Geophysical Research: Planets*, *126*, e2021JE006915. https://doi.org/10.1029/2021JE006915

Mittlefehldt, D. W., Gellert, R., van Bommel, S., Ming, D. W., Yen, A. S., Clark, B. C., et al. (2018). Diverse lithologies and alteration events on the rim of Noachian-aged Endeavour crater, Meridiani Planum, Mars: In situ compositional evidence. *Journal of Geophysical Research: Planets*, *123*(5), 1255–1306. https://doi.org/10.1002/2017JE005474

O'Connell-Cooper, C., Spray, J., Thompson, L., Gellert, R., Berger, J., Boyd, N., et al. (2017). APXS-derived chemistry of the Bagnold dune sands: Comparisons with Gale crater soils and the global Martian average. *Journal of Geophysical Research: Planets*, *121*(10), 1981–2003. https://doi.org/10.1002/2017JE005268

Rieder, R. G., Gellert, R., Anderson, R., Brückner, J., Clark, B. C., Dreibus, G., et al. (2004). Chemistry of rocks and soils at Meridiani Planum from the alpha particle X-ray spectrometer. *Science*, *306*(5702), 1746–1749. https://doi.org/10.1126/science.1104358

Saar, M., & Manga, M. (1999). Permeability—Porosity relationship in vesicular basalts. *Geophysical Research Letters*, *26*(1), 111–114. https://doi.org/10.1029/1998GL900256

Shao, Y., & Lu, H. (2000). A simple expression for wind erosion threshold friction velocity. *Journal of Geophysical Research*, *105*(D17), 22437–22443. https://doi.org/10.1029/2000JD900304

Silvestro, S., Chojnacki, M., Vaz, D. A., Cardinale, M., Yizhaq, H., & Esposito, F. (2020). Megaripple migration on Mars. *Journal of Geophysical Research: Planets*, *125*(8), e2020JE006446. https://doi.org/10.1029/2020JE006446

Soderblom, L. A., Anderson, R. C., Arvidson, R. E., Bell, J. F., Cabrol, N. A., Calvin, W., et al. (2004). Soils of Eagle crater and Meridiani Planum at the Opportunity rover landing site. *Science*, *306*(5702), 1723–1726. https://doi.org/10.1126/science.1105127

Squyres, S. W., Arvidson, R. E., Bell, J. F., III., Brückner, J., Cabrol, N. A., Calvin, W., et al. (2004). The Opportunity rover's Athena science investigation at Meridiani Planum, Mars. *Science*, *306*(5702), 1698–1703. https://doi.org/10.1126/science.1106171

Squyres, S. W., Arvidson, R. E., Bollen, D., Bell, J. F., III., Brückner, J., Cabrol, N. A., et al. (2006). Overview of the Opportunity Mars exploration rover mission to Meridiani Planum: Eagle crater to Purgatory ripple. *Journal of Geophysical Research*, *111*(E12), E12S12. https://doi.org/10.1029/2006JE002771

Sullivan, R., Baker, M., Newman, C., Turner, M., Schieber, J., Weitz, C., et al. (2022). The aeolian environment in Glen Torridon, Gale crater, Mars. *Journal of Geophysical Research: Planets*, *127*(8), e2021JE007174. https://doi.org/10.1029/2021JE007174

Sullivan, R., Banfield, D., Bell, J., Calvin, W., Fike, D., Golombek, M., et al. (2005). Aeolian processes at the Mars exploration rover Meridiani Planum landing site. *Nature*, *436*(7047), 58–61. https://doi.org/10.1038/nature03641

Sullivan, R., & Kok, J. F. (2017). Aeolian saltation on Mars at low wind speeds. *Journal of Geophysical Research: Planets*, *122*(10), 2111–2143. https://doi.org/10.1002/2017JE005275

Tholen, K., Pähtz, T., Yizhaq, H., Katra, I., & Kroy, K. (2022). Megaripple mechanics: Bimodal transport ingrained in bimodal sands. *Nature Communications*, *13*(1), 162. https://doi.org/10.1038/s41467-021-26985-3

Tirsch, D., Jaumann, R., Pacifici, A., & Poulet, F. (2011). Dark aeolian sediments in Martian craters: Composition and sources. *Journal of Geophysical Research*, *116*(E3), E03002. https://doi.org/10.1029/2009JE003562

Verma, S., Torres-Alvarado, I., & Velasco-Tapia, F. (2003). A revised CIPW norm. *Swiss Bulletin of Mineralogy and Petrology*, *83*, 197–216.

Wadell, H. A. (1932). Volume, shape and roundness of rock particles. *The Journal of Geology*, *40*(5), 443–451. https://doi.org/10.1086/623964

Waples, D. W., & Waples, J. S. (2004). A review and evaluation of specific heat capacities of rocks, minerals, and subsurface fluids. Part 1: Minerals and nonporous rocks. *Natural Resources Research*, *13*(2), 97–122. https://doi.org/10.1023/B:NARR.0000032647.41046.e7

Weitz, C. M., Anderson, R. C., Bell, J. F., III., Farrand, W. H., Herkenhoff, K. E., Johnson, J. R., et al. (2006). Soil grain analyses at Meridiani Planum, Mars. *Journal of Geophysical Research*, *111*(E12), E12S04. https://doi.org/10.1029/2005JE002541

Weitz, C. M., O'Connell-Cooper, C., Thompson, L., Sullivan, R. J., Baker, M., & Grant, J. A. (2022). The physical properties and geochemistry of grains on aeolian bedforms at Gale crater, Mars. *Journal of Geophysical Research: Planets*, *127*, e2021JE007061. https://doi.org/10.1029/2021JE007061

Weitz, C. M., Sullivan, R. J., Lapotre, M. G. A., Rowland, S. K., Grant, J. A., Baker, M., & Yingst, R. A. (2018). Sand grain sizes and shapes in eolian bedforms at Gale crater, Mars. *Geophysical Research Letters*, *45*(18), 9471–9479. https://doi.org/10.1029/2018GL078972

Wentworth, C. K. (1922). A scale of grade and class terms for clastic sediments. *The Journal of Geology*, *30*(5), 377–392. https://doi.org/10.1086/622910

Yingst, R. A., Crumpler, L., Farrand, W. H., Li, R., Cabrol, N. A., & Neakrase, L. D. (2008). Morphology and texture of particles along the Spirit rover traverse from sol 450 to sol 745. *Journal of Geophysical Research*, *113*(E12), E12S41. https://doi.org/10.1029/2008JE003179

Yu, Q., Bagas, L., Yang, P., & Zhang, D. (2019). GeoPyTool: A cross-platform software solution for common geological calculations and plots. *Geoscience Frontiers*, *10*(4), 1437–1447. https://doi.org/10.1016/j.gsf.2018.08.001

Zheng, J. (2023). Particle roundness and sphericity computation. *MATLAB Central File Exchange*. https://www.mathworks.com/matlabcentral/fileexchange/60651-particle-roundness-and-sphericity-computation

Zheng, J., & Hryciw, R. D. (2016). Roundness and sphericity of soil particles in assemblies by computational geometry. *Journal of Computing in Civil Engineering*, *30*(6), 04016021. https://doi.org/10.1061/(ASCE)CP.1943-5487.0000578